SACLANTCEN Memorandum
SM - 157

# SACLANT ASW RESEARCH CENTRE MEMORANDUM

## CONSISTENCY TESTS OF ACOUSTIC PROPAGATION MODELS

by

FINN B. JENSEN and WILLIAM A. KUPERMAN



1 MARCH 1982



NORTH ATLANTIC TREATY ORGANIZATION

LA SPEZIA, ITALY

SACLANTCEN MEMORANDUM SM-157

NORTH ATLANTIC TREATY ORGANIZATION

SACLANT ASW Research Centre
Viale San Bartolomeo 400, I-19026 San Bartolomeo (SP), Italy.

tel: national 0187 560940
international + 39 187 560940

telex: 271148 SACENT I

# CONSISTENCY TESTS OF ACOUSTIC PROPAGATION MODELS

by

Finn B. Jensen and William A. Kuperman

1 March 1982

*This memorandum has been prepared within the SACLANTCEN Underwater Research Division as part of Project 19.*

O.F. HASTRUP
Division Chief

TABLE OF CONTENTS


| | | Page |
|---|---|---|
| ABSTRACT | | 1 |
| INTRODUCTION | | 1 |
| 1 | TEST CASE 1: RANGE-DEPENDENT SURFACE DUCT | 2 |
| 2 | TEST CASE 2: RANGE-INDEPENDENT ENVIRONMENT WITH DIFFERENT BOTTOM SPEEDS | 4 |
| 3 | TEST CASE 3: RANGE-INDEPENDENT SHALLOW-WATER ENVIRONMENT | 5 |
| 4 | TEST CASE 4: PROPAGATION OVER A SLOPING BOTTOM WITH A SEDIMENT LAYER | 7 |
| SUMMARY AND CONCLUSIONS | | 9 |
| REFERENCES | | 10 |
| APPENDIX A – MATHEMATICAL FOUNDATION OF ACOUSTIC MODELS | | 49 |
| APPENDIX B – DESCRIPTION OF THE FOUR COMPUTER MODELS | | 71 |


List of Figures


| | | |
|---|---|---|
| 1. | Inter-model comparison for case 1A. | 11 |
| 2. | Inter-model comparison for case 1B. | 13 |
| 3. | Inter-model comparison for case 1C. | 15 |
| 4. | Contoured propagation loss from PE model going from deep to shallow duct. | 17 |
| 5. | Contoured propagation loss from PE model going from shallow to deep duct. | 19 |
| 6. | Reciprocity test for PE model for case 1B. | 21 |
| 7. | Inter-model comparison for case 2A. | 23 |
| 8. | Inter-model comparison for case 2B. | 25 |
| 9. | Inter-model comparison for case 2C. | 27 |
| 10. | Inter-model comparison for case 3A. | 29 |
| 11. | Inter-model comparison for case 3B. | 31 |
| 12. | Contoured propagation loss from PE model for case 3B. | 33 |
| 13. | Ray trace for case 4. | 35 |
| 14. | Inter-model comparison for case 4A. | 37 |
| 15. | Inter-model comparison for case 4B. | 39 |
| 16. | Comparison of three range-dependent model results for case 4B. | 41 |
| 17. | Inter-model comparison for case 4C. | 43 |

List of Figures (Cont'd) Page

18. Inter-model comparison for case 4D. 45
19. Comparison of three range-dependent model results for case 4D. 47

A.1 Techniques for solving the wave equation. 49
A.2 FFP integrand plot for case 2A (full spectrum). 61
A.3 FFP integrand plot for case 2A (discrete spectrum). 63
A.4 Mode-amplitude functions for case 2A. 65
A.5 Inter-model comparison for case 2A (near field). 67
A.6 Inter-model comparison for case 2A (far field). 69

# CONSISTENCY TESTS OF ACOUSTIC PROPAGATION MODELS

by

Finn B. Jensen and William A. Kuperman

## ABSTRACT

Three wave-theory models (NM, FFP, PE) and one ray model are applied to four different ocean environments: a range-dependent surface duct, a deep-water environment with a homogeneous bottom, a shallow-water environment with a homogeneous bottom, and a sloping-bottom environment with a layered bottom. The consistency among the acoustic models is clearly demonstrated through the agreement between model results for the various test problems.

## INTRODUCTION

In this report we present the results of an inter-model comparison for which four different underwater acoustic environments were studied. Three wave-theory models were used: Normal Mode (NM), Fast Field Program (FFP), and Parabolic Equation (PE). This study is an outgrowth of the Parabolic Equation Workshop <1> held at the US Naval Ocean Research and Development Activity (NORDA) in April 1981. The test cases were provided by the Numerical Modelling Division of NORDA and various participants used these test cases for their PE models; comparisons between PE results were presented at the Workshop. We also did the test cases with the PE, but in addition we ran most of the cases with other wave models in order to obtain independent solutions to the four problems. On occasion we even ran a ray model for completeness. The result is a rather complete set of test cases, each of which has been studied with various models. Where there is essentially full agreement among the three wave models for the complicated environments (which do not lend themselves to analytic solutions), we believe that the answers presented are the correct solutions to the wave equation since the numerical algorithms used are totally different for the three models (and the PE model even uses an approximation of the wave equation!).

In the next four chapters we present the NORDA test cases together with numerical results from the various models. We then summarize the results of this inter-model comparison and give some numerical parameters and associated computer times for NM and PE solutions to the four test problems. Appendix A outlines the mathematical basis of the various acoustic models and Appendix B provides a brief description (with appropriate references) of the specific computer codes used.

## 1 TEST CASE 1: RANGE-DEPENDENT SURFACE DUCT

This test problem has a range-dependent sound speed and consists of profile 1A from 0 to 20 km, a transition from profile 1A to 1B over the range interval 20 to 30 km, and profile 1B from 30 to 50 km, as shown in Table 1.

Figures 1, 2, and 3* display the result for the three receiver depths. The NM and FFP solutions are applicable only in the range-independent region, that is, up to the dashed line at range 20 km. Beyond 20 km the difference between the FFP and PE solutions indicates the effect of range dependence on computed propagation losses. We see that at ranges of less than 20 km there is excellent agreement between the results of the three models, the greatest disagreement occurring in the nearfield where the FFP should work best (see App. A). Note though, that in the nearfield the PE and FFP have better agreement with each other than they do with the NM calculation. Of course the NM calculation does not include the nearfield contribution, but it is interesting to note how well the PE performs in the nearfield.

The main difficulty in running this problem with the PE model was to avoid acoustic returns from the lower boundary of the truncated z-domain. We obtained stable results by moving the boundary to a depth of 4000 m, and by introducing an artificial absorption in the lower 1000 m of that domain. To obtain discrete normal-mode solutions for this case, which essentially is a "continuous spectrum" problem, we had to introduce an artificial bottom with a speed of 1500 m/s (equal to maximum speed in the surface duct). By moving this bottom to a depth of 4000 m we obtained stable NM solutions to cases 1A and 1B, with the trapped "continuous mode" in the surface duct now being simulated through a set of 36 discrete modes. However, for the receiver below the surface channel (case 1C) we found no efficient manner in which the discrete NM model could simulate the "continuous spectrum" problem.

The conclusion from Figs. 1 to 3 is that the PE gives the correct result in the range-independent part of the environment and because of the mathematical nature of the PE solution (see App. A) there is no reason to believe that the accuracy of this solution diminishes in the mildly range-dependent region.

Contouring the PE transmission-loss results over depth and range provides further insight into the basic propagation mechanisms involved in this case. Figure 4 shows propagation from the deep to the shallow surface duct with the source in the duct (25 m). The contour lines indicate that there is essentially one mode propagating in the duct out to ranges of about 25 km. Here the mode is cut off and sound is leaving the duct as indicated by the dashed arrow. Such mode cut-off and radiation into the bottom has been studied in detail elsewhere <2>. If we reverse the propagation direction we get the result shown in Fig. 5. Here we have placed the source below the shallow duct (SD = 250 m). We see that sound is propagating with high losses in the duct out to ranges of about 25 km. Here the duct widens and sound becomes trapped in the duct; consequently propagation conditions improve (longer spacing between contour lines).

*All figures are at the end of the text.

TABLE 1

TEST CASE 1

Frequency = 25 Hz
Source depth (SD) = 25 m
Receiver depths (RD) = 25, 250 and 400 m
Max range = 50 km

Profile 1A

| Depth (m) | Sound speed (m/s) | Density ($g/cm^3$) | Attenuation (dB/km) |
|---|---|---|---|
| 0 | 1480 | 1. | 0. |
| 300 | 1500 | 1. | 0. |
| 1000 | 1460 | 1. | 0. |
| ∞ | 1460 | 1. | 0. |

Profile 1B

| Depth (m) | Sound speed (m/s) | Density ($g/cm^3$) | Attenuation (dB/km) |
|---|---|---|---|
| 0 | 1492.38 | 1. | 0. |
| 200 | 1505.71 | 1. | 0. |
| 300 | 1500.00 | 1. | 0. |
| 1000 | 1460.00 | 1. | 0. |
| ∞ | 1460.00 | 1. | 0. |

The profile in the transition interval is range dependent between depths of 0 and 300 m and is given by:

$$h(r) = 300 - 10\,(r-20)$$

$$C_s(r) = 1480 + 1.238\,(r-20)$$

$$C_d(r) = 1500 + 0.571\,(r-20),$$

where

$h(r)$ is the depth of the duct in metres

$C_s(r)$ is the sound speed (in m/s) at zero depth

$C_d(r)$ is the sound speed (in m/s) at the bottom of the duct

$r$ is horizontal range in km.

Plots:

Separate plots from 0 to 50 km for each of the three receiver depths.

The results in Figs. 4 and 5 naturally lead to a test for reciprocity in the PE approximation to the wave equation. The result for case 1B is shown in Fig. 6; the reciprocal case for the deep to shallow with SD = 25 m and RD =250 m is shallow to deep and SD = 250 m and RD = 25 m. That is, not only is the direction of propagation reversed but the source and receiver depths must also be interchanged. Reciprocity for range-dependent propagation requires that only at the final range of propagation must the answers be the same, and indeed they are at a range of 50 km. The calculations are not the same throughout the total range for a range-dependent environment because the environments are different for the two cases. For example, at 20 km, the answers are far apart because in one case we are propagating in the shallow duct (no trapping of sound) and in the other case, in the deep duct (one mode trapped). Figure 6, however, demonstrates that reciprocity is included in the parabolic-equation method.

## 2 TEST CASE 2: RANGE-INDEPENDENT ENVIRONMENT WITH DIFFERENT BOTTOM SPEEDS

This test problem has a range-independent environment with a bi-linear sound speed in the water column and a half-space bottom. It consists of three parts, A, B and C, with different sound-speed profiles, as shown in Table 2.

TABLE 2

TEST CASE 2

Frequency = 25 Hz
Source depth (SD) = 500 m
Receiver depth (RD) = 500 m
Max range = 20 km
Density = 1 g/cm$^3$
Attenuation = 0 dB/km

| Depth (m) | Sound speed (m/s) | | |
|---|---|---|---|
| | Part A | Part B | Part C |
| 0 | 1500 | 1500 | 1500 |
| 1000 | 1520 | 1520 | 1520 |
| 1500 | 1563 | 1744 | 1971 |
| ∞ | 1563 | 1744 | 1971 |

Plots:

Separate plots from 10 to 20 km for each of the three parts.

Since this case is a range-independent environment we know that NM and FFP are applicable, with the caveat that the discrete NM solution will not give an adequate description of the nearfield (see App. A). The results for the three cases are shown in Figs. 7 to 9. Note first the excellent agreement between FFP and NM, indicating that we have the true solution to the wave equation. Next notice that the agreement between PE and NM/FFP deteriorates with increasing bottom speed *even though the approximate* levels are correct. With increasing bottom speed the maximum angle of propagation (with respect to the horizontal) increases and so does the number of propagating modes, and both factors affect the accuracy of the PE solution. For cases A, B, and C the angles are 15°, 30°, and 40° respectively, and the number of modes are 11, 22, and 28.

The PE is a narrow-angle approximation to the wave equation (see App. A) and accurate results are obtained only for propagation angles of less than 15 to 20° with the horizontal. Moreover, there is an inherent phase error in the PE that results in slightly different spatial interference patterns than those calculated by an exact solution to the wave equation (NM or FFP). This phase error becomes more evident as the number of modes increases. In this study we have employed a correction procedure <3> that should reduce PE phase errors, particularly in deep-water type environments. For case 2A (Fig. 7), where propagation angles are less than 15°, the PE follows the correct interference pattern quite accurately, indicating that the phase-correction procedure works properly. However, with increasing angle of propagation (Figs. 8 and 9) the accuracy of the PE solution deteriorates, and though some prominent features are retained (including a correct mean level), a component of randomness is seen in the PE interference pattern for these wide-angle cases.

We showed for case 1 (Ch. 1) that the PE includes the "continuous spectrum" contribution. In Appendix A we discuss this aspect in more detail with reference to case 2A, showing that the PE substantially agrees with the nearfield FFP result, the classical Lloyd mirror pattern.

## 3 TEST CASE 3: RANGE-INDEPENDENT SHALLOW-WATER ENVIRONMENT

This test problem has a range-independent environment and consists of an isovelocity water column over an isovelocity half-space bottom. There are two parts, A and B, with different source and receiver depths, as shown in Table 3.

Again we see that for both of these cases (Figs. 10 and 11) we have agreement between FFP and NM and hence we have the wave-theory solution. For this environment the steepest angle of propagation is around 20° and hence the narrow-angle approximation should not affect the accuracy of the PE solution, at least not for source and receiver at mid-depth. Since the PE phase-correction procedure <3> is not effective for this environment with heavy bottom interaction, we have tried to minimize phase errors in the PE solution by an appropriate choice of reference speed (see App. A). The reference speed should be chosen to match the phase velocity of the most important mode <4>. For case 3A, with source and receiver at mid-depth, sound is mainly propagating in the lower-order modes (the total number of modes is 11). By choosing a PE reference speed of 1500 m/s,

which is close to the phase velocity of the first mode (1500.6 m/s), we obtained the good agreement between PE and NM/FFP solutions shown in Fig. 10.

For case 3B, with source and receiver near the bottom boundary, higher-order modes are significantly excited, making the interference pattern more complex than for case 3A. We see in Fig. 11 that the PE solution does not precisely track the true interference pattern. Nevertheless, observe the agreement at the large destructive interference null at a range of 7 km. This agreement was obtained using a PE reference speed of 1550 m/s, which is a mean value for the phase speeds of this problem. (The difference between FFP and NM solutions around 7 km is attributed to inaccuracies in the computations; phase accuracy is crucial for achieving the degree of cancellation between modes shown here). Note in Fig. 11 that the average level for the PE solution is a little too low. This is probably due to the narrow-angle approximation, which affects propagation amplitudes at steeper angles.

The most interesting feature of this test problem is the large destructive interference null for case 3B. The transmission-loss contours of Fig. 12 created by the PE model show the spatial extent of the null region around 7 km. A special check on the adequacy of the gaussian beam for initializing the PE solution was done for case 3; we obtained identical results whether starting with a normal-mode field or with the gaussian beam, even for the source close to the bottom.

TABLE 3

TEST CASE 3

| | |
|---|---|
| Frequency | = 250 Hz |
| Water depth | = 100 m |
| Sound speed in water | = 1500 m/s |
| Density in water | = 1.0 g/cm$^3$ |
| Density in bottom | = 1.2 g/cm$^3$ |
| Attenuation in water | = 0 |
| Bottom attenuation | = 0.5 dB/$\lambda$ |
| Bottom sound speed | = 1590 m/s |
| Max range | = 10 km |

| | Part A: | Part B |
|---|---|---|
| Source depth | 50 m | 99.5 m |
| Receiver depth | 50 m | 99.5 m |

Plots:

Separate plots from 5 to 10 km for each of the two parts.

## 4 TEST CASE 4: PROPAGATION OVER A SLOPING BOTTOM WITH A SEDIMENT LAYER

This problem has a range-independent sound speed in the water column, a range-dependent bottom depth and a simple geoacoustic bottom that is tied to the sound speed at the bottom of the water column, as shown in Table 4.

This is a fairly complicated environment, where the steepest propagation angles are around 40°. Hence the narrow-angle approximation could cause inaccuracies in the PE results, particularly at short ranges where steep bottom-bounce paths are most important. No phase correction was applied to the PE solution; we chose a reference speed of 1500 m/s. The total number of modes for this case is 77. The range-averaged propagation-loss curves were produced using a sliding rectangular window (equal weighting of all samples).

Figure 13 shows the bathymetry, the layering, and a ray trace of the waterborne paths to indicate the type of long-range propagation expected. Figures 14 and 15 show good agreement in the levels obtained by the NM and FFP calculations. In particular, the 20 km smoothed results (Fig. 15) are virtually identical for FFP and NM. Figures 14 and 15 also indicate good agreement with the PE solution. The slightly lower PE levels for ranges less than 25 km are probably caused by an incorrect handling of bottom-bounce paths (not traced in Fig. 13 to keep the plot simple). These steep propagation paths will carry only little energy after a few bounces off the bottom. Note in Fig. 15 that NM and FFP solutions are applicable only out to a range of 150 km. Beyond this range we have bathymetric changes that are included only in the PE solution. We see that for this particular receiver depth there is no effect of the changing water depth on propagation loss between 150 and 190 km. Then there is a sharp fall-off in the PE curve as the receiver moves into the bottom.

Figure 16 compares the PE result with range-dependent ray theory and adiabatic mode theory. Neither the adiabatic mode nor the ray calculation could be made for the full range, since these particular models were not set up to have a receiver in the bottom. For the ray-theory calculation the sediment was taken to have a density of one and no attenuation. This was done so that the sediment layer could be treated as part of the sound-speed profile in the water column. In general there is good agreement among the models. The slightly higher level of the ray-theory result beyond 75 km is because no attenuation was included in the sediment.

Results for test case 4C are shown in Fig. 17, where PE is compared against adiabatic mode theory. There is agreement between levels, but, as we expected, the interference pattern is slightly shifted because of phase errors. Figure 18 displays test 4D results and compares NM, FFP and PE. Note that ranges less than 150 km correspond to a range-independent environment where NM and FFP are applicable. Beyond 150 km comparison of the PE result with the NM/FFP results indicates the difference between constant depth and sloping-bottom propagation. The initial increase in level up the slope is a geometrical effect of the decrease in water depth. In the shallow-water region beyond 200 km the increased interaction with the bottom results in increased losses with range.

Finally, Fig. 19 indicates that the PE result for this case is in good agreement with adiabatic mode theory while ray theory again gives levels that are too high because no attenuation was included in the sediment layer.

# TABLE 4

## TEST CASE 4

Frequency = 25 Hz
Source depth = 600 m
Receiver depths = 150 and 700 m
Max range = 250 km

Water column parameters

| Depth (m) | Sound speed (m/s) | Density ($g/cm^3$) | Attenuation (dB/km) |
|---|---|---|---|
| 0 | 1539.3 | 1. | 0. |
| 30 | 1539.8 | 1. | 0. |
| 200 | 1534.2 | 1. | 0. |
| 600 | 1502.4 | 1. | 0. |
| 700 | 1495.4 | 1. | 0. |
| 800 | 1491.8 | 1. | 0. |
| 1000 | 1488.0 | 1. | 0. |
| 1100 | 1487.5 | 1. | 0. |
| 1200 | 1487.9 | 1. | 0. |
| 3410 | 1525.0 | 1. | 0. |

| Range | Bottom depth |
|---|---|
| | Bottom depth |
| 0-150 km | Constant 3410 m |
| 150-200 km | Linearly decreasing from 3410 m to 200 m with increasing range |
| 200-250 km | Constant 200 m |

Sediment:

Sound speed at top of sediment is:

$$CT_s(r) = 0.975 \times C_w(r),$$

where $C_w(r)$ is the sound speed at the bottom of the water column.

Sound speed at the bottom of sediment is:

$$CB_s(r) = 1.305 \times CT_s(r)$$

Sediment thickness = 454 m (constant in range)

Attenuation = 0.375 dB/km = 0.015 dB/km/Hz

Density = 1.5 $g/cm^3$

Basement:

Sound speed = $CB_s(r)$

Attenuation = 0.

Density = 2.5 $g/cm^3$

Example: At a range of 200 km,

Water depth = 200 m

$C_w$(200 km) = 1534.2 m/s

$CT_s$(200 km) = 1495.8 m/s

$CB_s$(200 km) = 1952.1 m/s

Basement depth = 654 m

Plots:

For 700 m receiver depth:
case A - 1 km average from 10 to 50 km
case B - 20 km average from 0 to 250 km

For 150 m receiver depth:
case C - 1 km average from 175 to 225 km
case D - 20 km average from 0 to 250 km

## SUMMARY AND CONCLUSIONS

Considering the completeness of this study (four models compared) and the realistic ocean environmental descriptions contained in the four test problems, it seems likely that the results given in this report could constitute a set of benchmark tests for other propagation models in the future. With that prospect in view we have attempted to include as much useful information as possible on the various test cases and on the acoustic models. In this spirit and to facilitate the reproduction of the results in this report, we have listed in Table 5 representative numerical parameters and associated computer times for both the normal mode and the PE model. The necessary sampling in depth, $\Delta z$, for obtaining stable numerical solutions is seen to be of the same order of magnitude for both models. The sampling in range, $\Delta r$, has significance for numerical accuracy only in the PE model. The transform size given for each test problem can be used to compute the total depth domain ($H_{max}$) used in the PE computation, i.e. $H_{max} = \Delta z \cdot 2^N$. The computer times relate to a UNIVAC 1100/60. We see that the PE model is particularly slow when there is heavy bottom interaction (cases 3 and 4). We did not attempt to optimize the FFP runs. However, an FFP calculation is generally slower than a mode computation.

TABLE 5

NUMERICAL PARAMETERS AND ASSOCIATED COMPUTER TIMES (UNIVAC 1100/60) FOR MODE AND PE SOLUTIONS TO THE FOUR TEST CASES

| | | NM | PE |
|---|---|---|---|
| Case 1 | $\Delta z$ (m) | 5.0 | 3.9 |
| | $\Delta r$ (m) | 100 | 100 |
| | $2^N$ | - | 1024 |
| | t (min) | 1 | 3 |
| Case 2 | $\Delta z$ (m) | 7.5 | 11.2 |
| | $\Delta r$ (m) | 25 | 25 |
| | $2^N$ | - | 256 |
| | t (min) | <1 | 1 |
| Case 3 | $\Delta z$ (m) | 0.5 | 0.26 |
| | $\Delta r$ (m) | 10 | 2 |
| | $2^N$ | - | 1024 |
| | t (min) | <1 | 30 |
| Case 4 | $\Delta z$ (m) | 8.5 | 5.2 |
| | $\Delta r$ (m) | 500 | 100 |
| | $2^N$ | - | 1024 |
| | t (min) | 2 | 15 |

To sum up, we have presented numerical calculations for the NORDA test cases. The consistency among normal mode, FFP, and PE (and ray theory) has been clearly demonstrated and cases of disagreement are well understood. It was never a straightforward procedure to obtain correct answers from either of the models employed in this study. Unfortunately the state-of-development of scientific propagation models is such that considerable experience with a given model is necessary in order to get meaningful results. However, of the models used here (see App. B), the ray and normal-mode programs definitely have reached a higher level of refinement and automation than the other two models and they are therefore the easiest to run. The PE model and particularly the FFP model require at present considerable insight into the specific numerical schemes in order to produce meaningful propagation-loss predictions.

## REFERENCES

1. DAVIS, J., WHITE, D. and CAVANAUGH, R. Proceedings of PE workshop. Bay St. Louis, Miss., US Naval Ocean Research and Development Activity (in preparation).

2. JENSEN, F.B. and KUPERMAN, W.A. Sound propagation in a wedge-shaped ocean with a penetrable bottom. Journal Acoustical Society America 67, 1980: 1564-1566.

3. BROCK, H.K., BUCHAL, R.N. and SPOFFORD, C.W. Modifying the sound speed profile to improve the accuracy of the parabolic equation technique. Journal Acoustical Society America 62, 1977: 543-552.

4. MCDANIEL, S.T. Propagation of normal mode in the parabolic approximation. Journal Acoustical Society America 57, 1975: 307-311.

# FIGURES

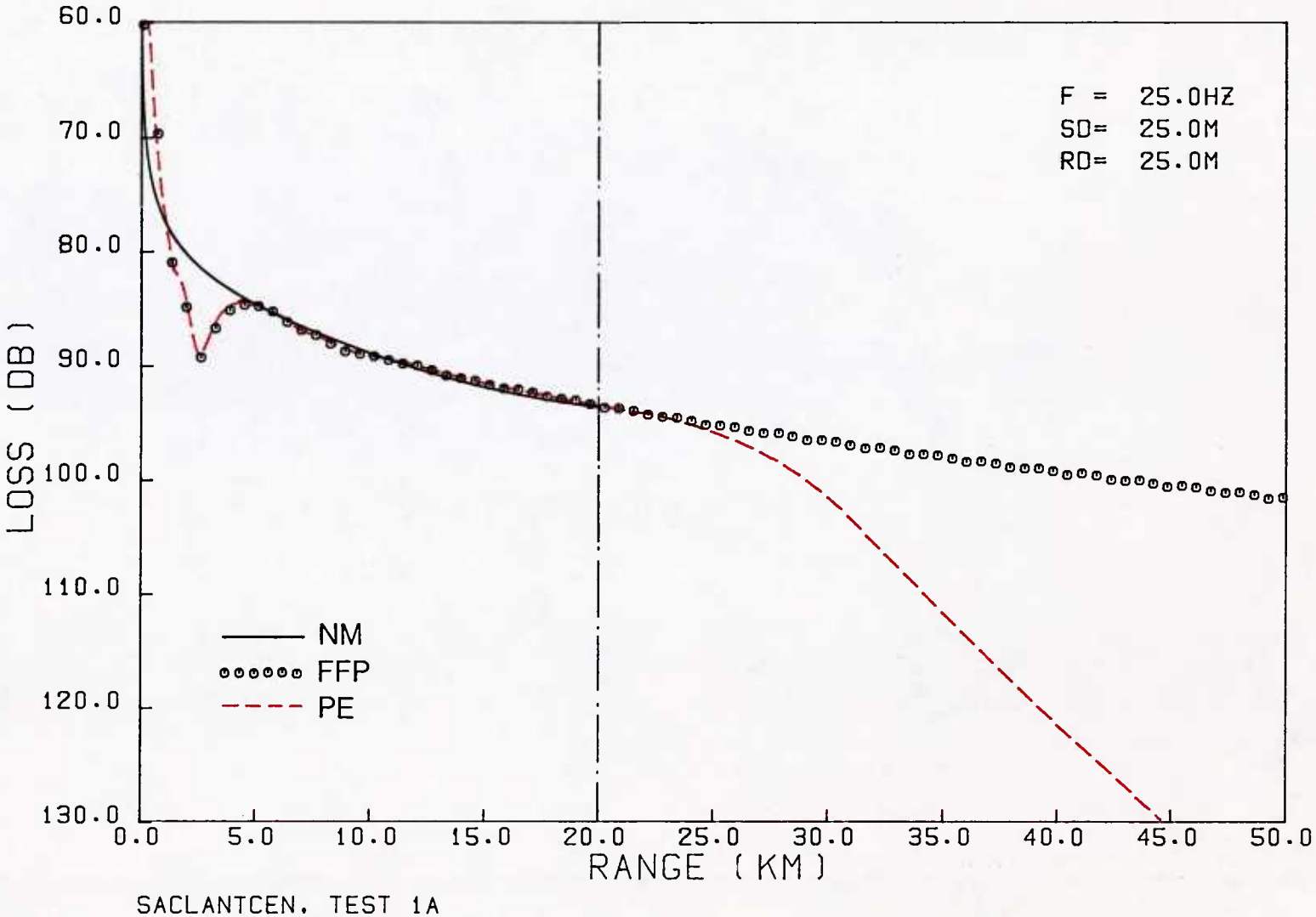


*FIG. 1 INTER-MODEL COMPARISON FOR CASE 1A*

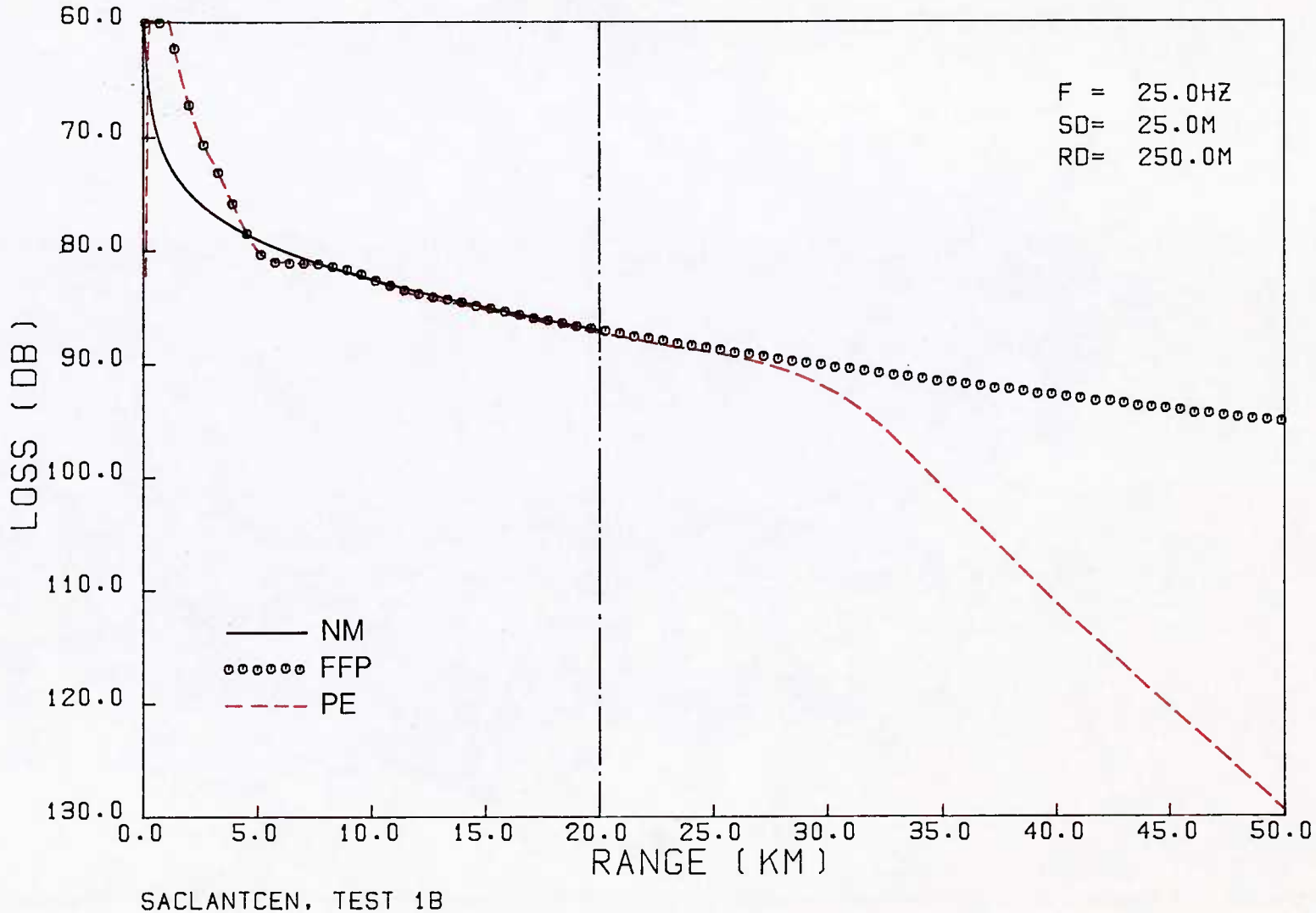


*FIG. 2 INTER-MODEL COMPARISON FOR CASE 1B*

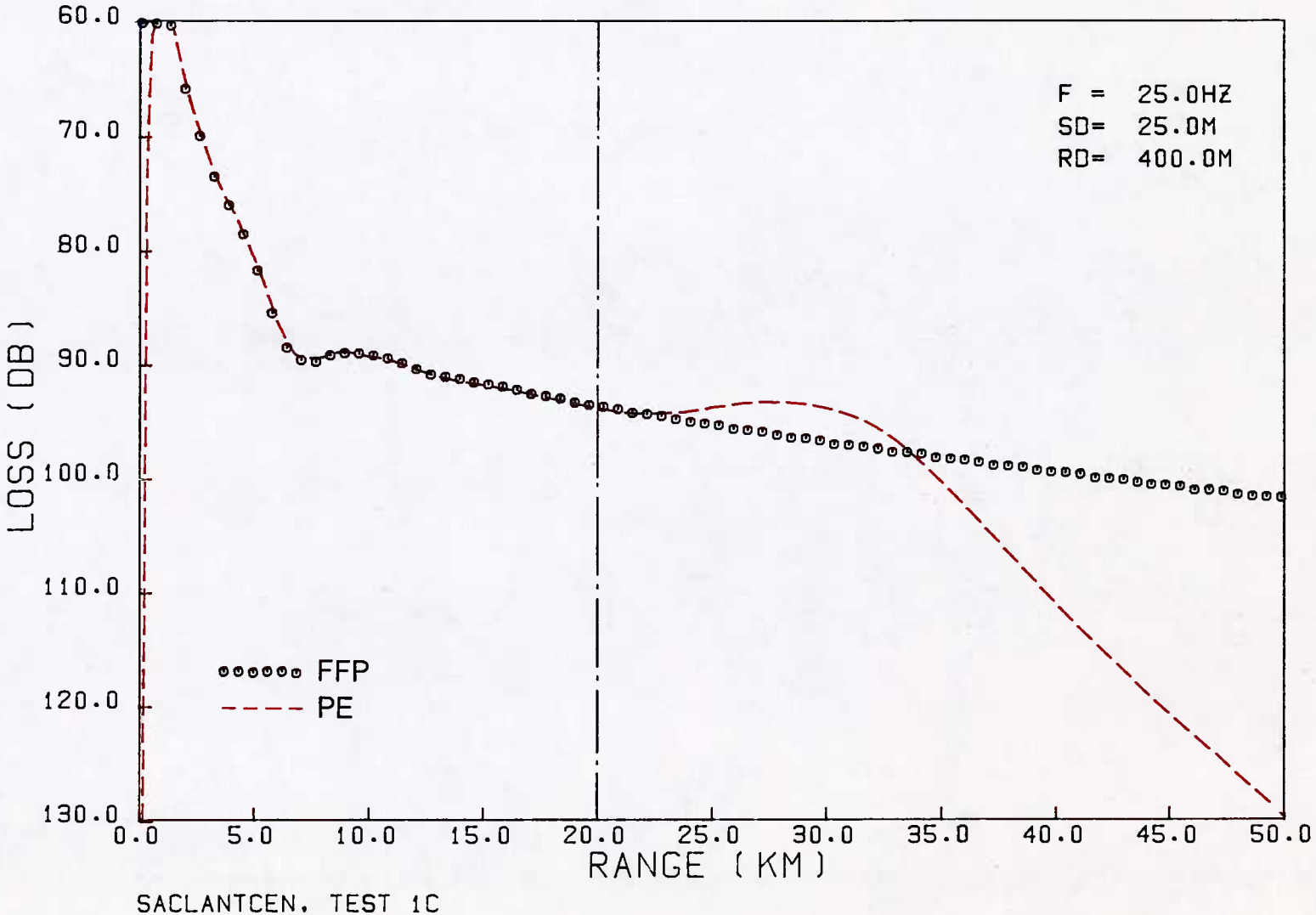


*FIG. 3 INTER-MODEL COMPARISON FOR CASE 1C*

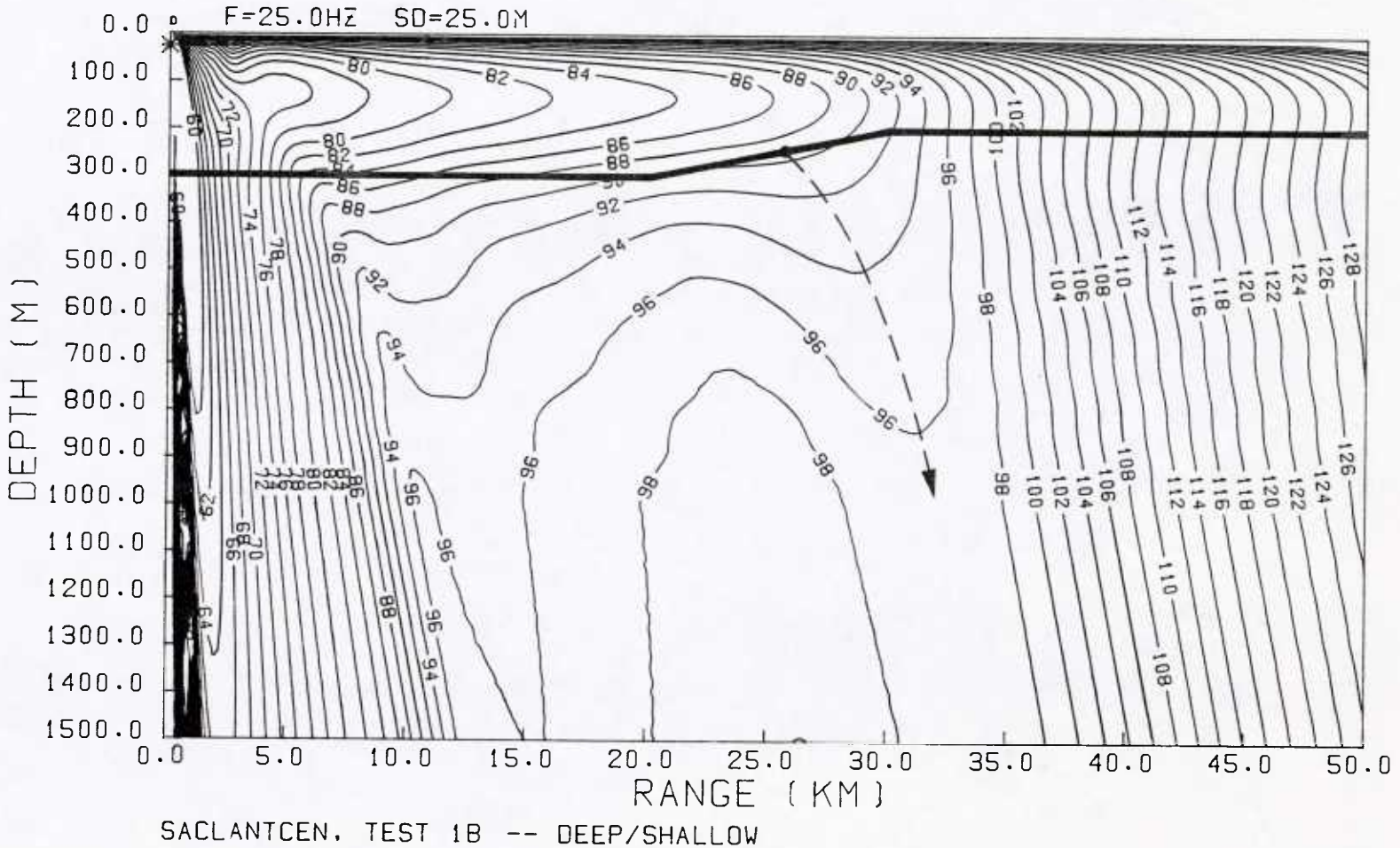


*FIG. 4 CONTOURED PROPAGATION LOSS FROM PE MODEL GOING FROM DEEP TO SHALLOW DUCT*

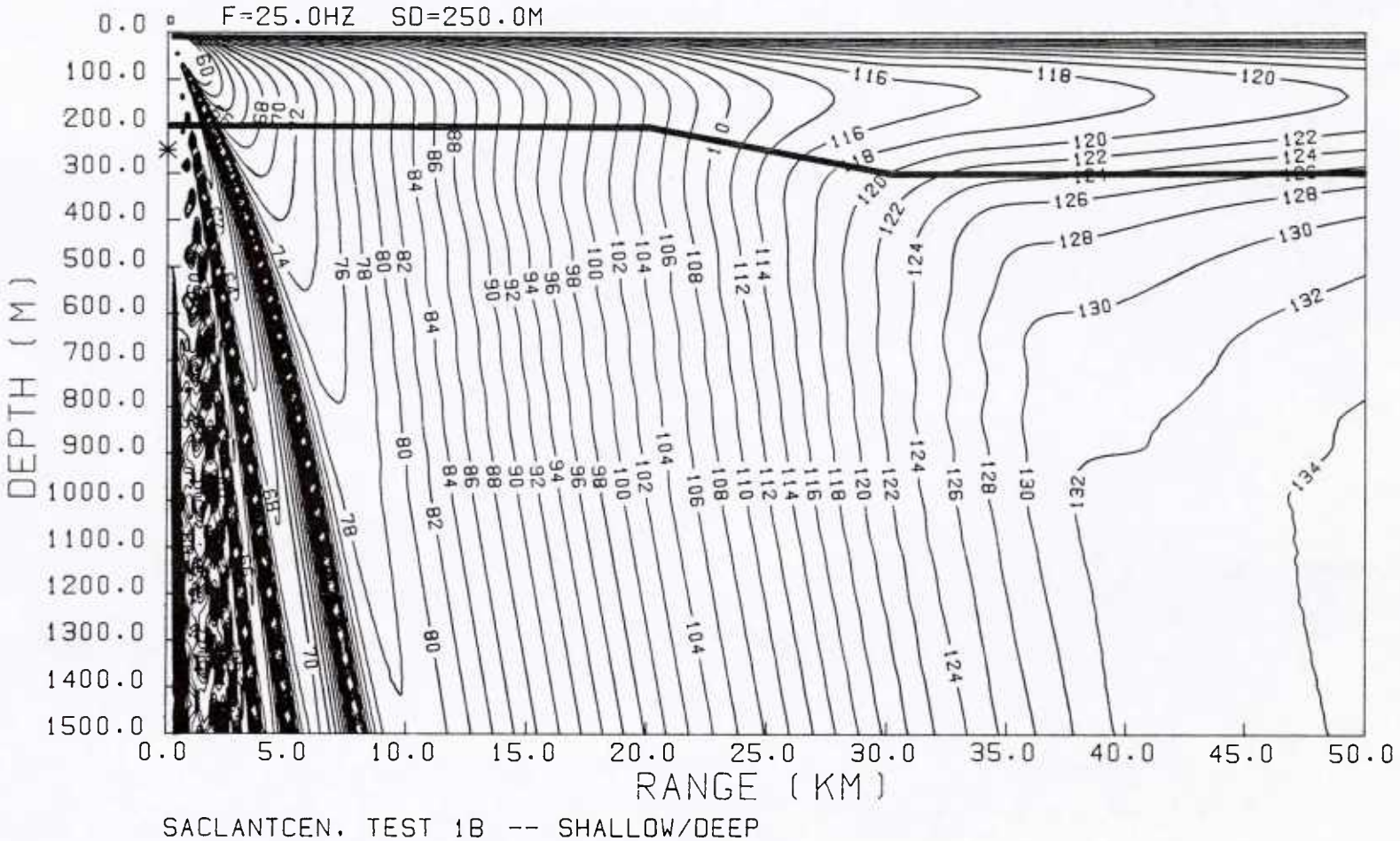


*FIG. 5 CONTOURED PROPAGATION LOSS FROM PE MODEL GOING FROM SHALLOW TO DEEP DUCT*

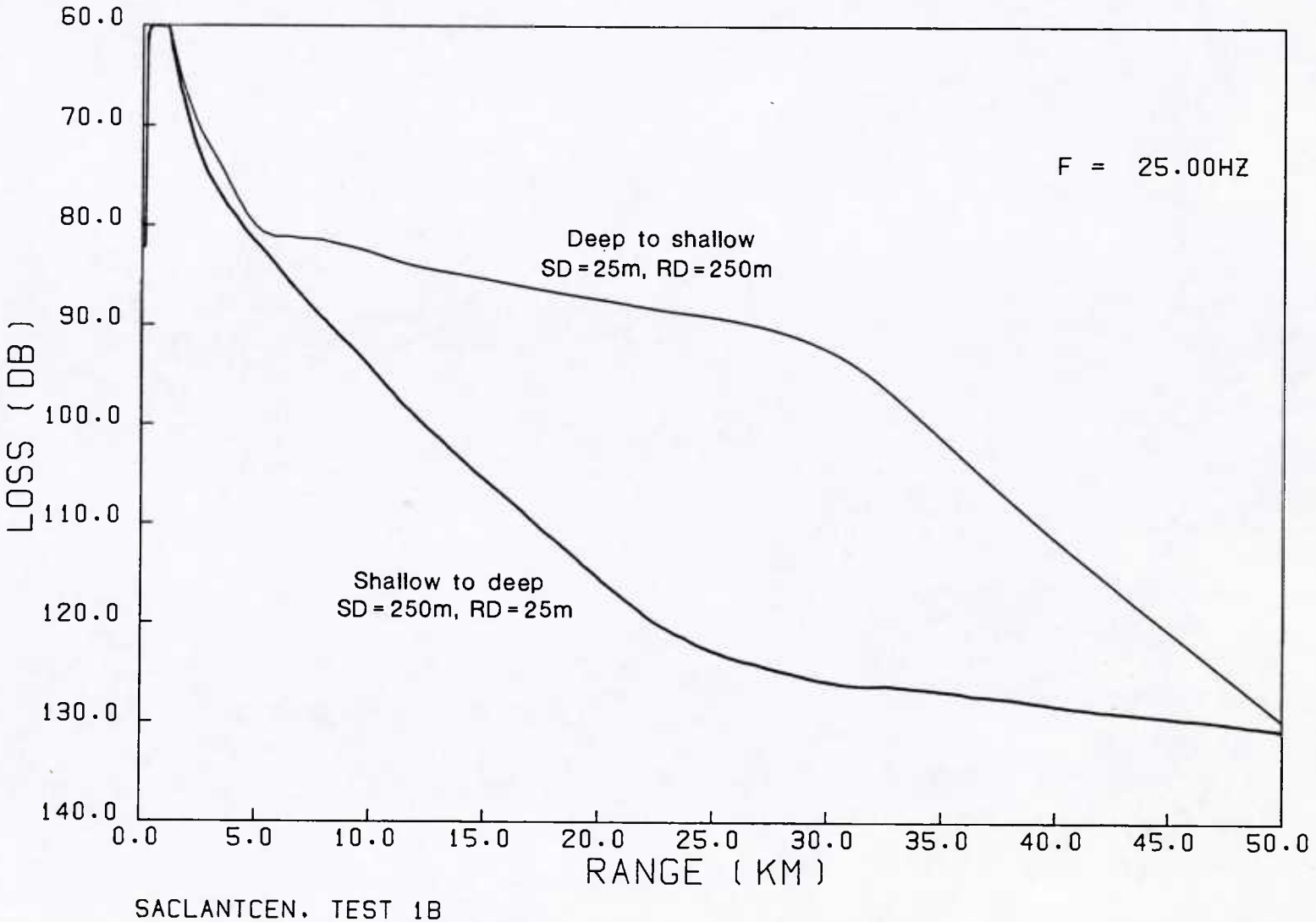


*FIG. 6 RECIPROCITY TEST FOR PE MODEL FOR CASE 1B*

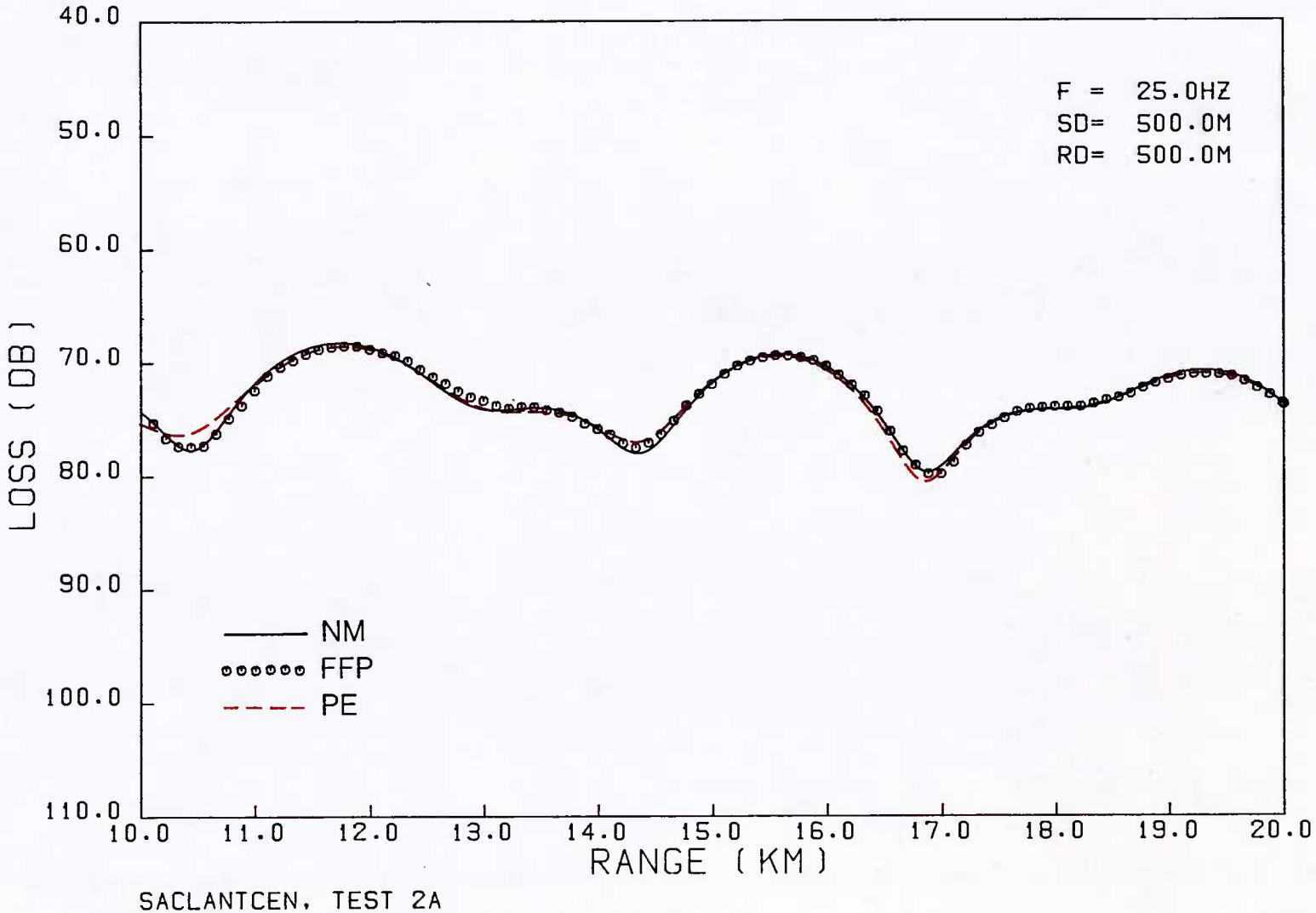


*FIG. 7 INTER-MODEL COMPARISON FOR CASE 2A*

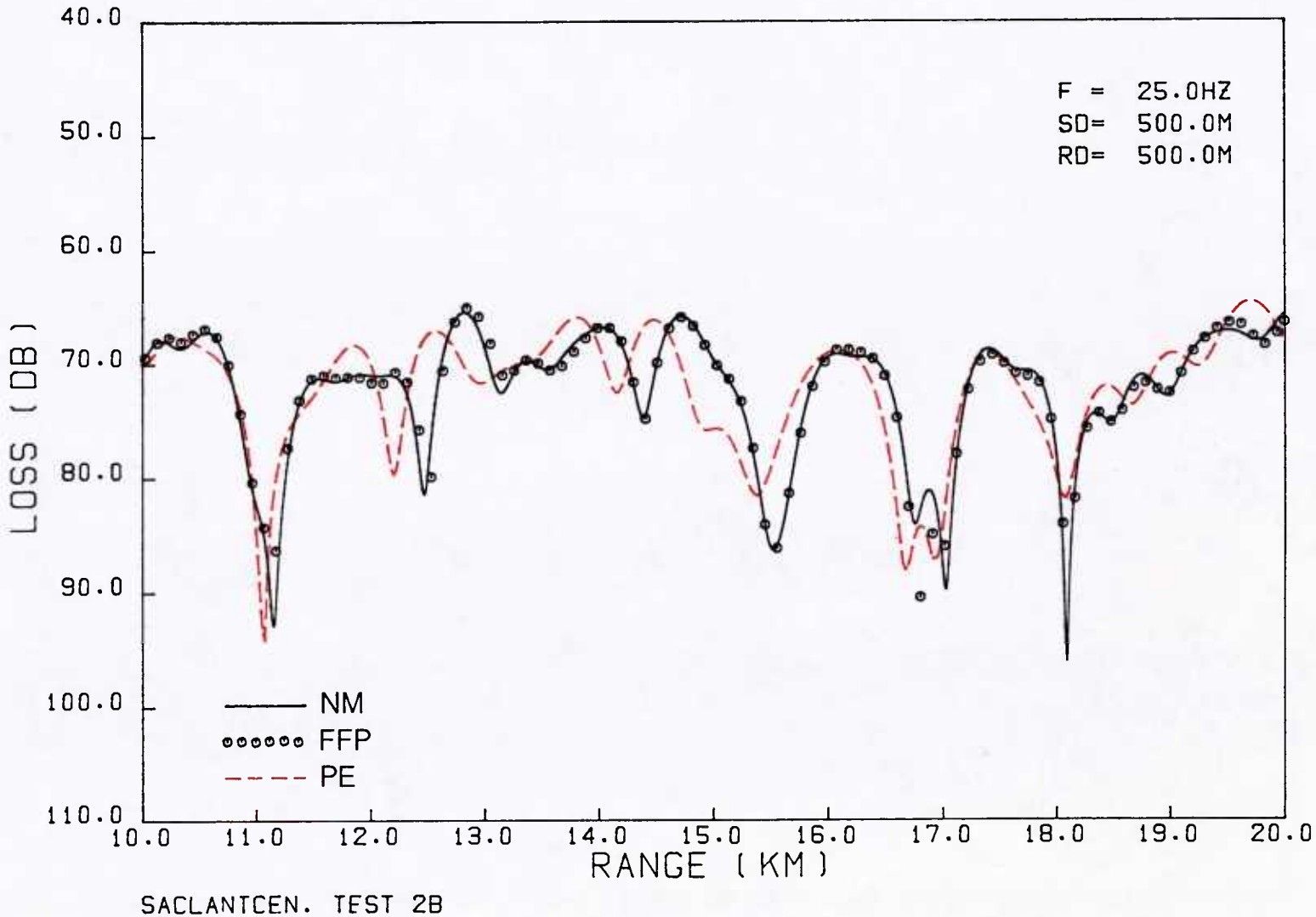


*FIG. 8 INTER-MODEL COMPARISON FOR CASE 2B*

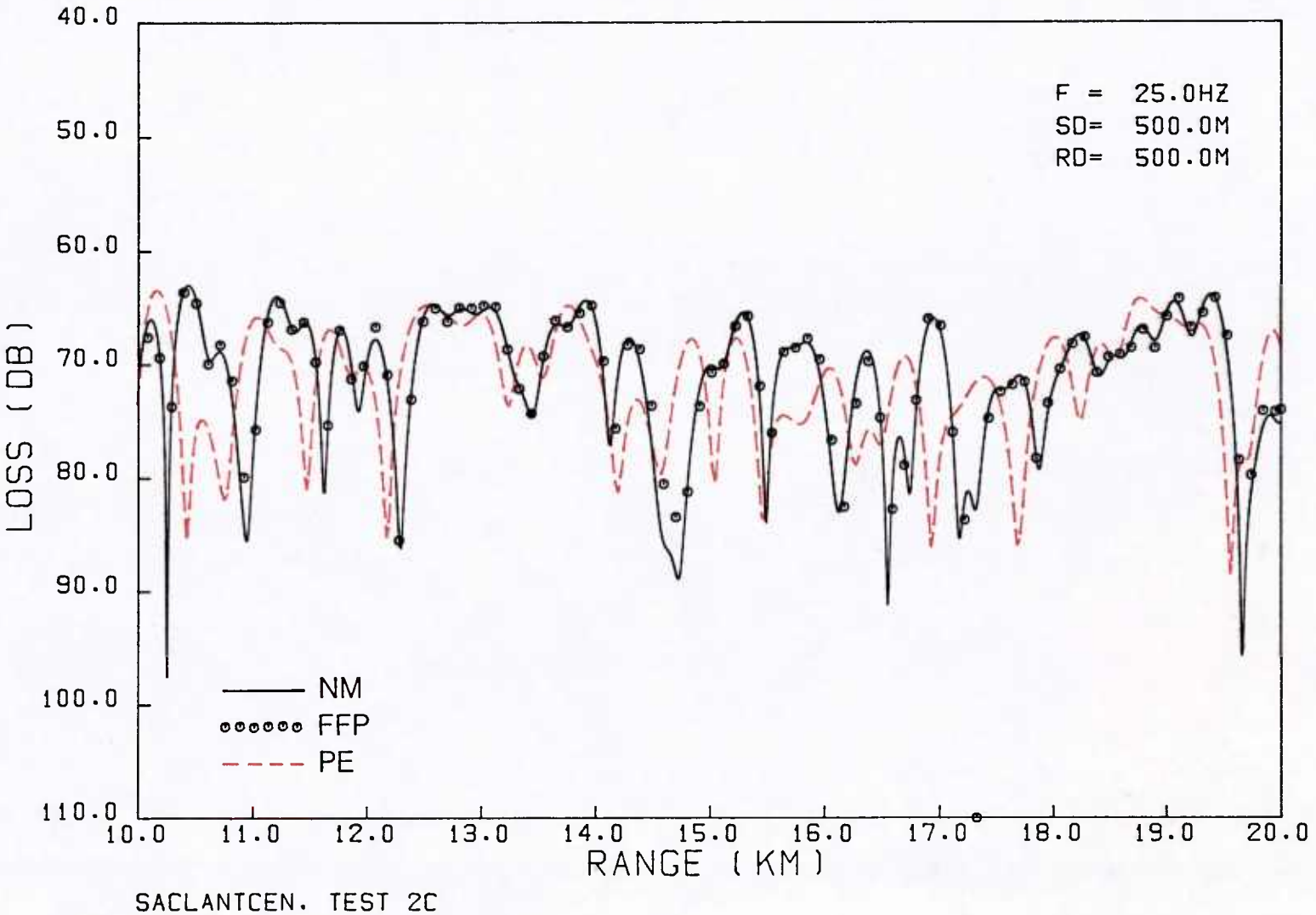


*FIG. 9 INTER-MODEL COMPARISON FOR CASE 2C*

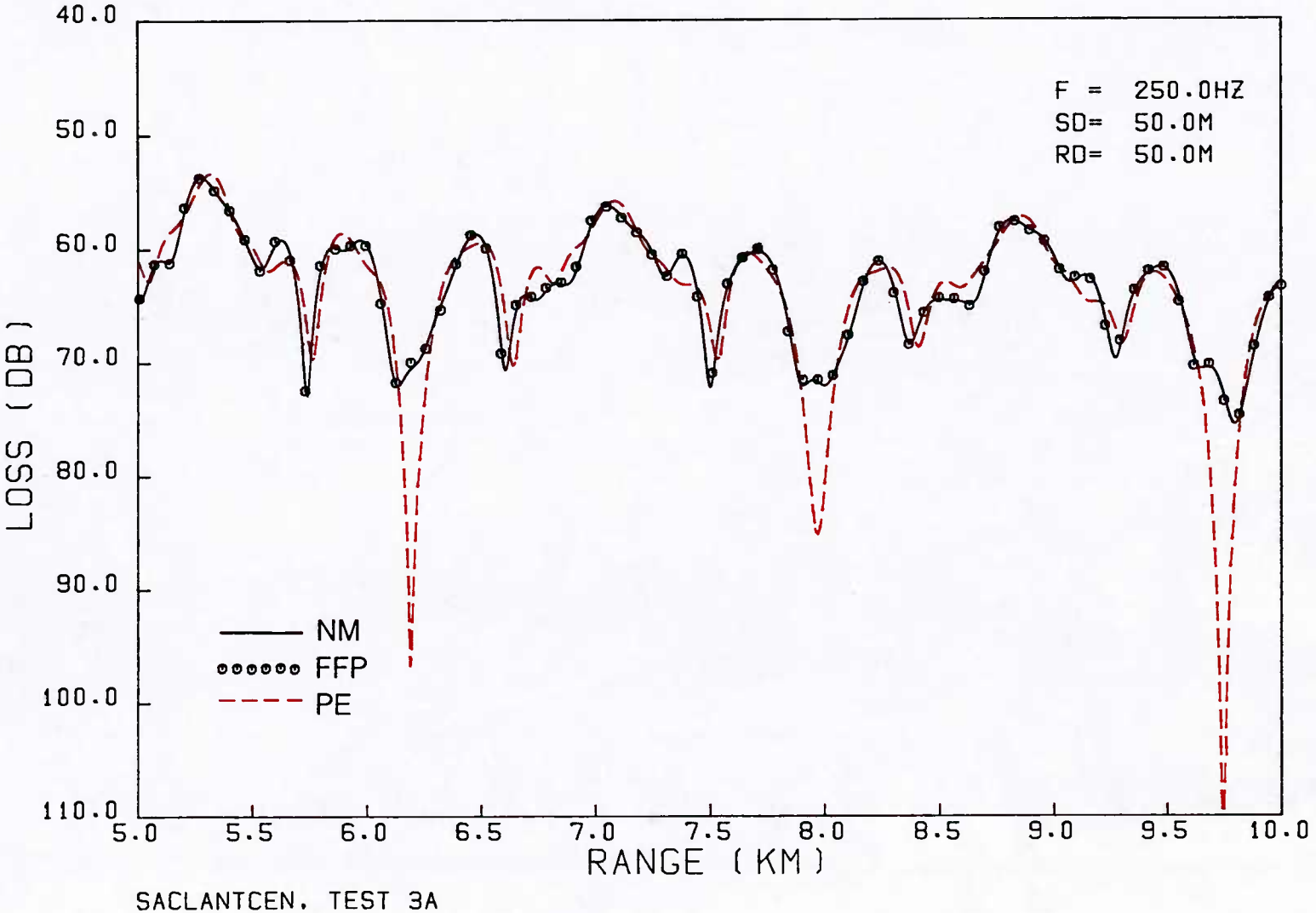


*FIG. 10 INTER-MODEL COMPARISON FOR CASE 3A*

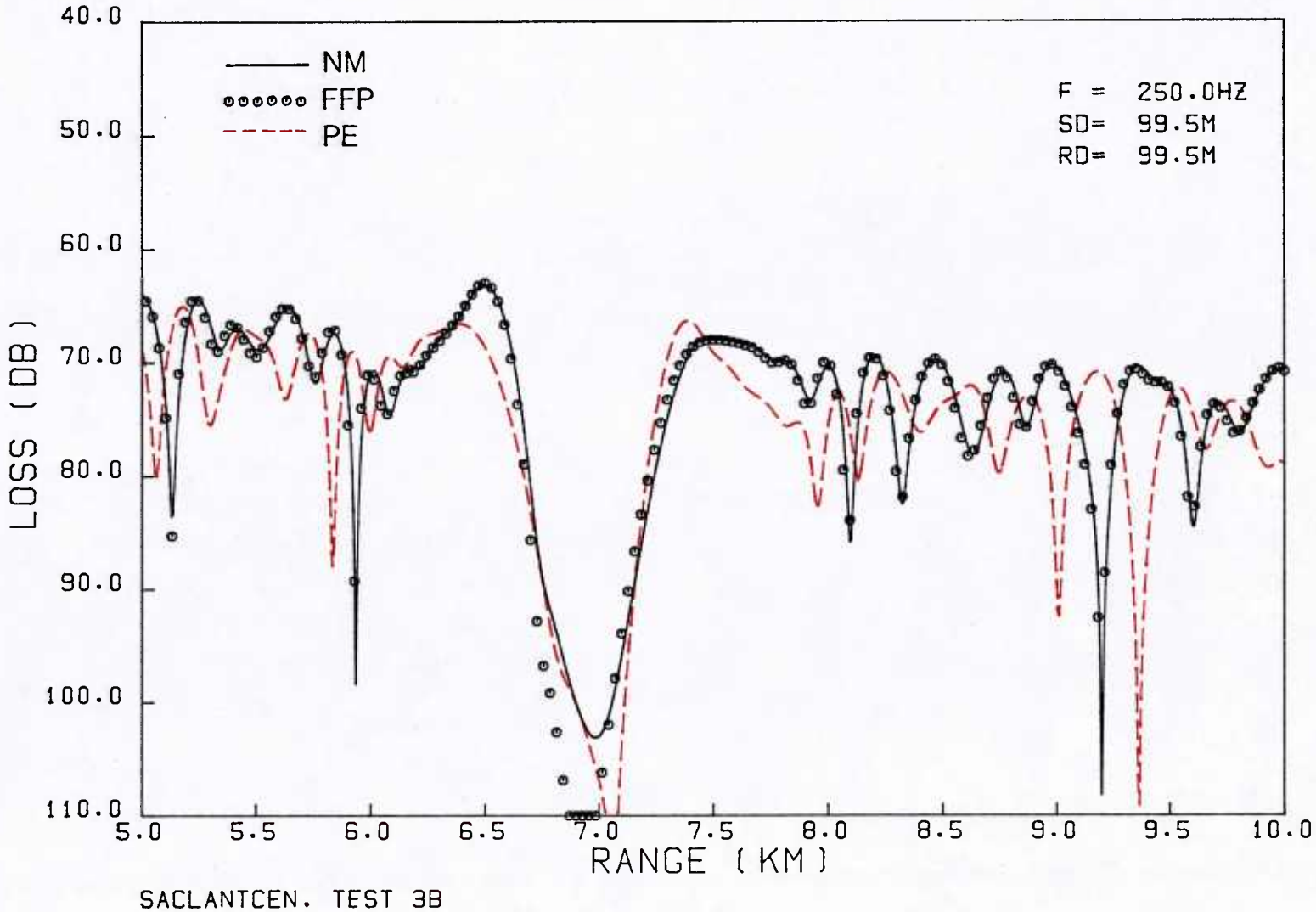


*FIG. 11 INTER-MODEL COMPARISON FOR CASE 3B*

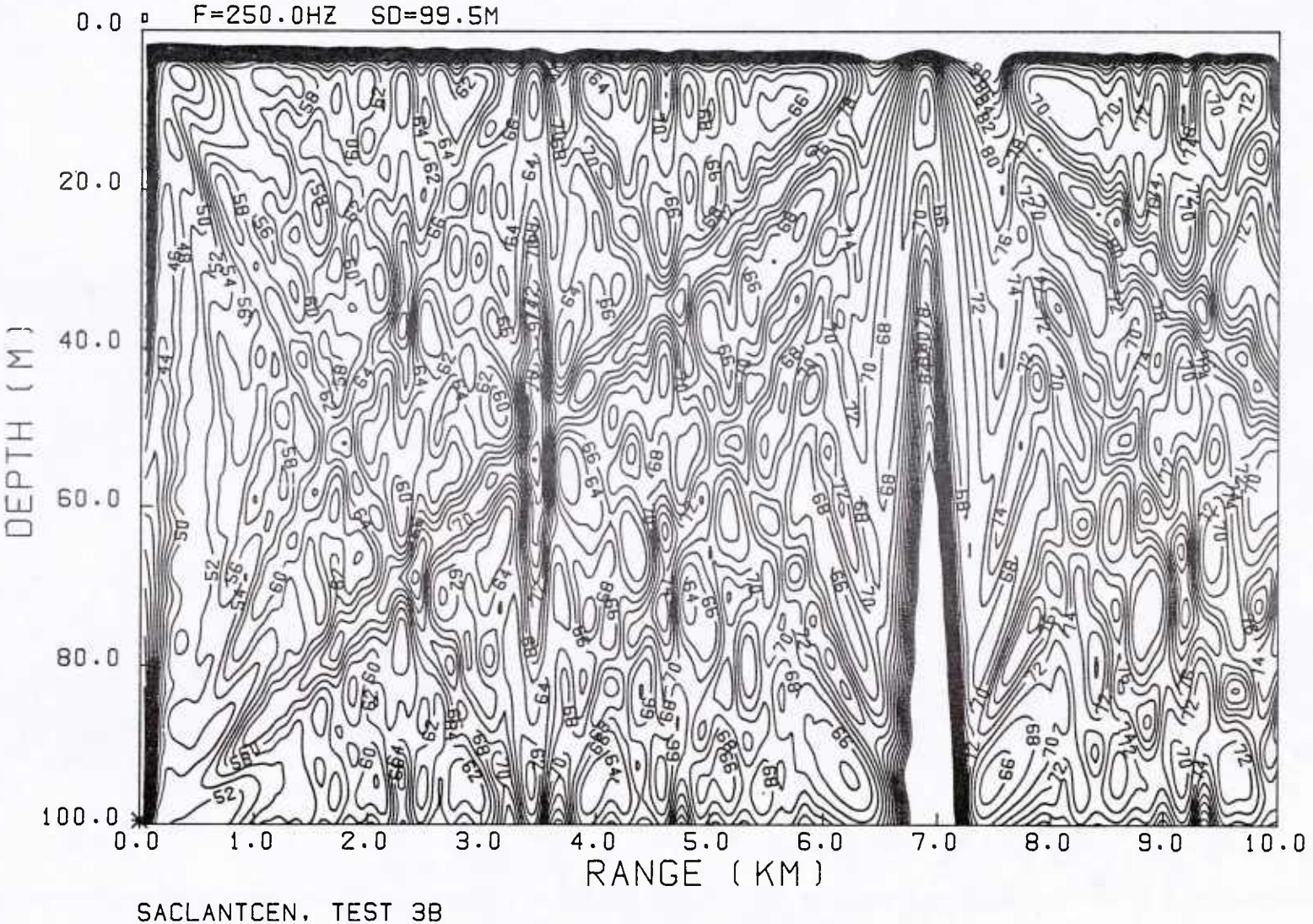


*FIG. 12 CONTOURED PROPAGATION LOSS FROM PE MODEL FOR CASE 3B*

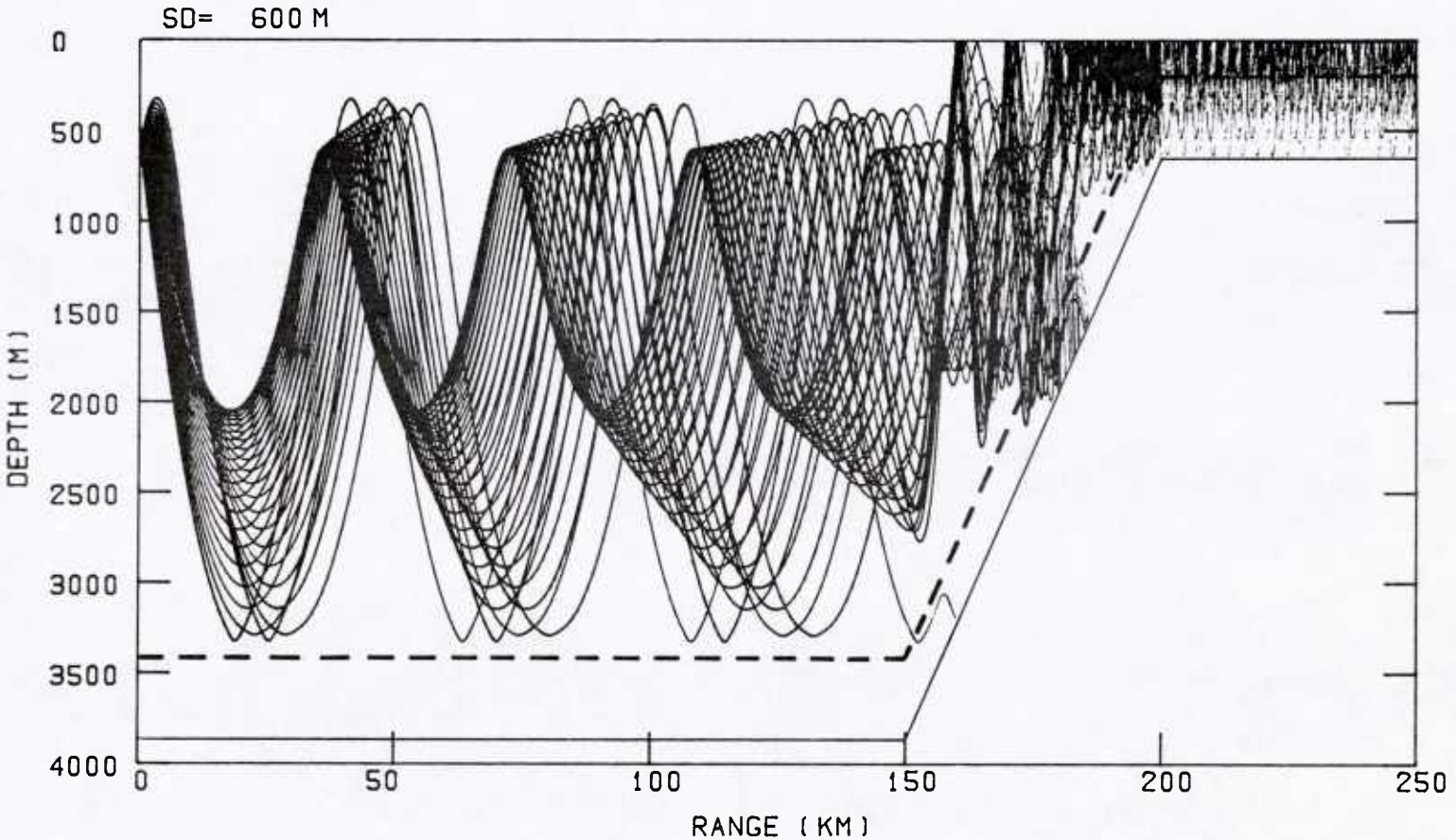


*FIG. 13 RAY TRACE FOR CASE 4. The dashed line indicates the water/sediment interface*

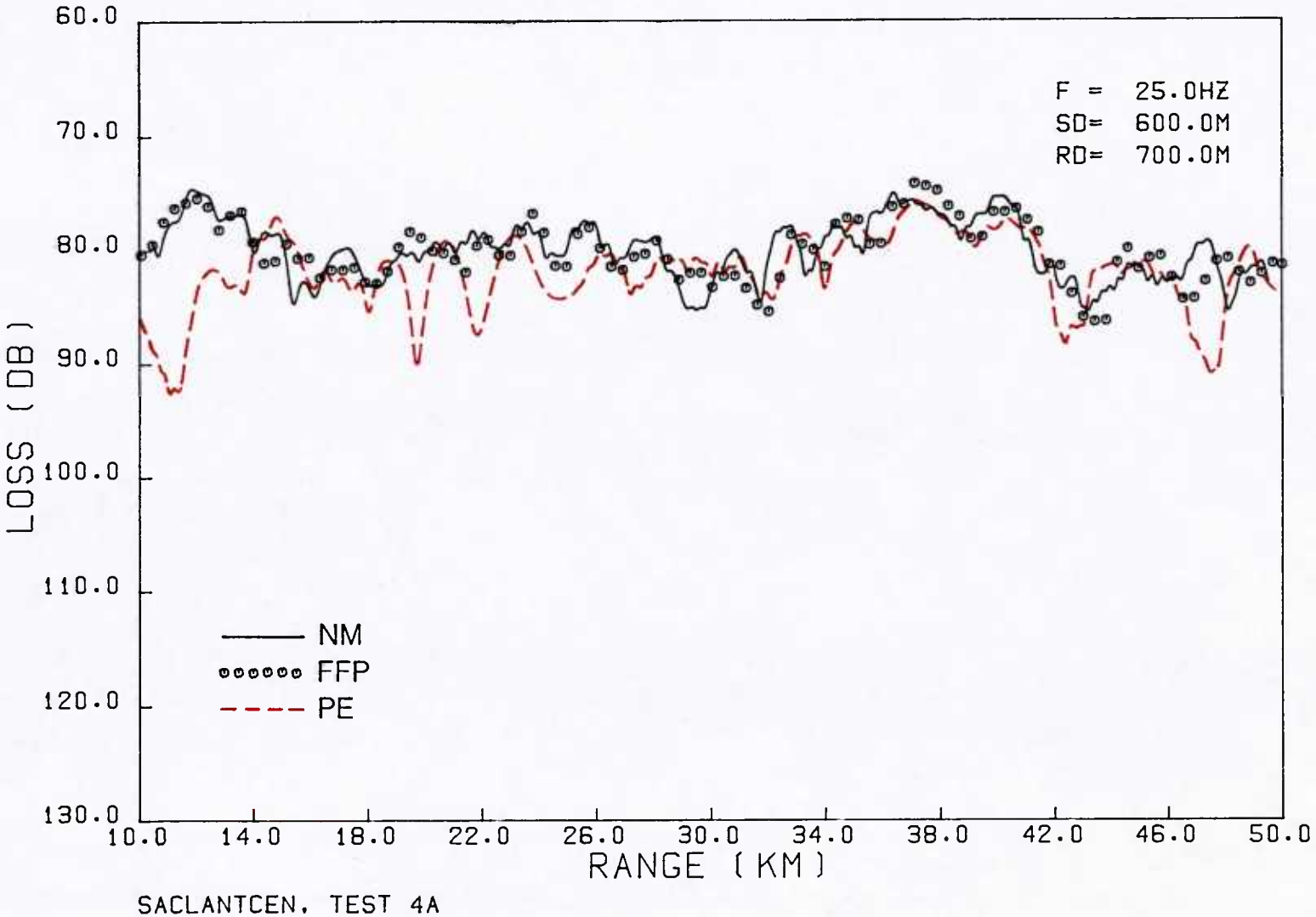


*FIG. 14 INTER-MODEL COMPARISON FOR CASE 4A*

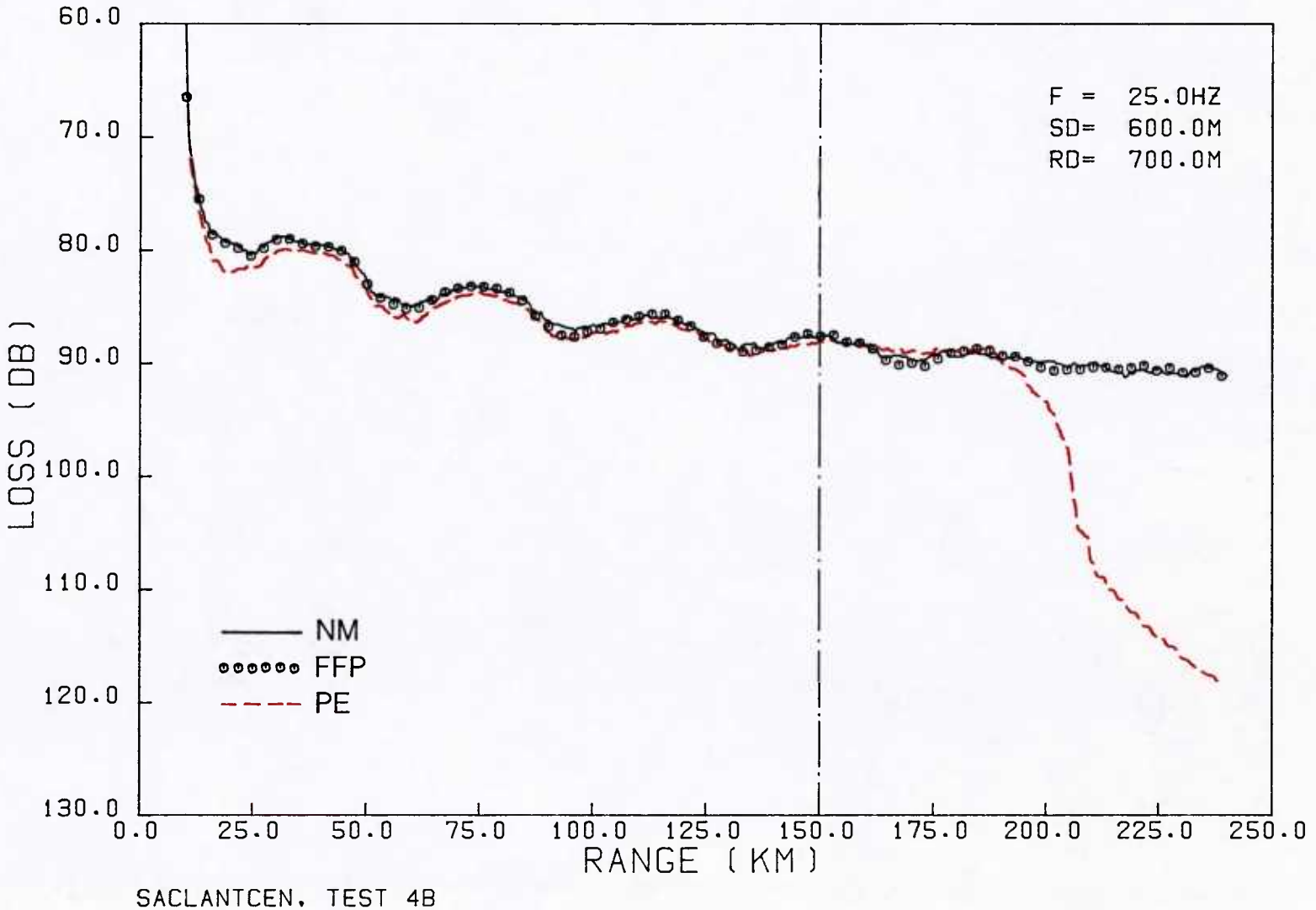


*FIG. 15 INTER-MODEL COMPARISON FOR CASE 4B*

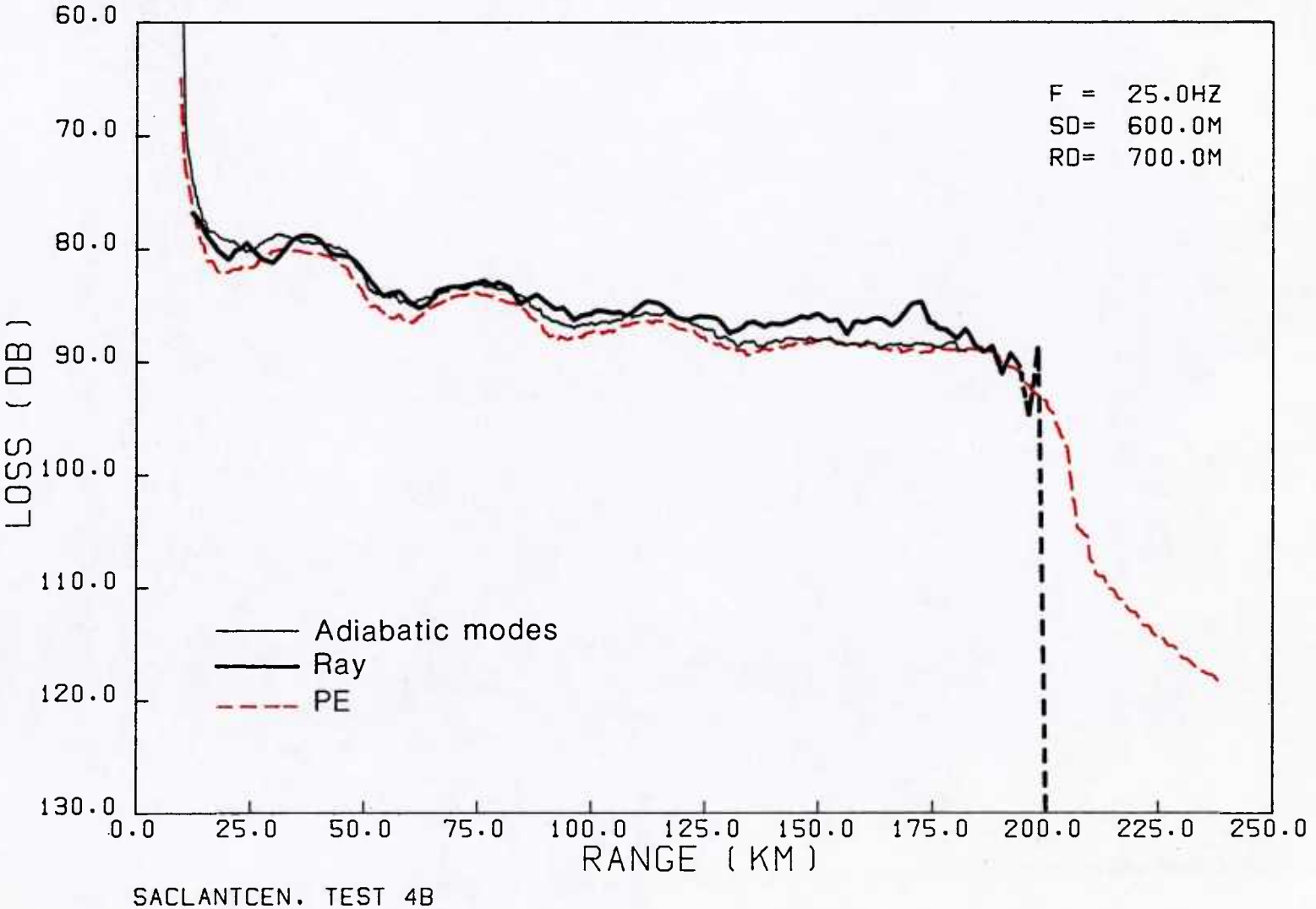


*FIG, 16 COMPARISON OF THREE RANGE-DEPENDENT MODEL RESULTS FOR CASE 4B*

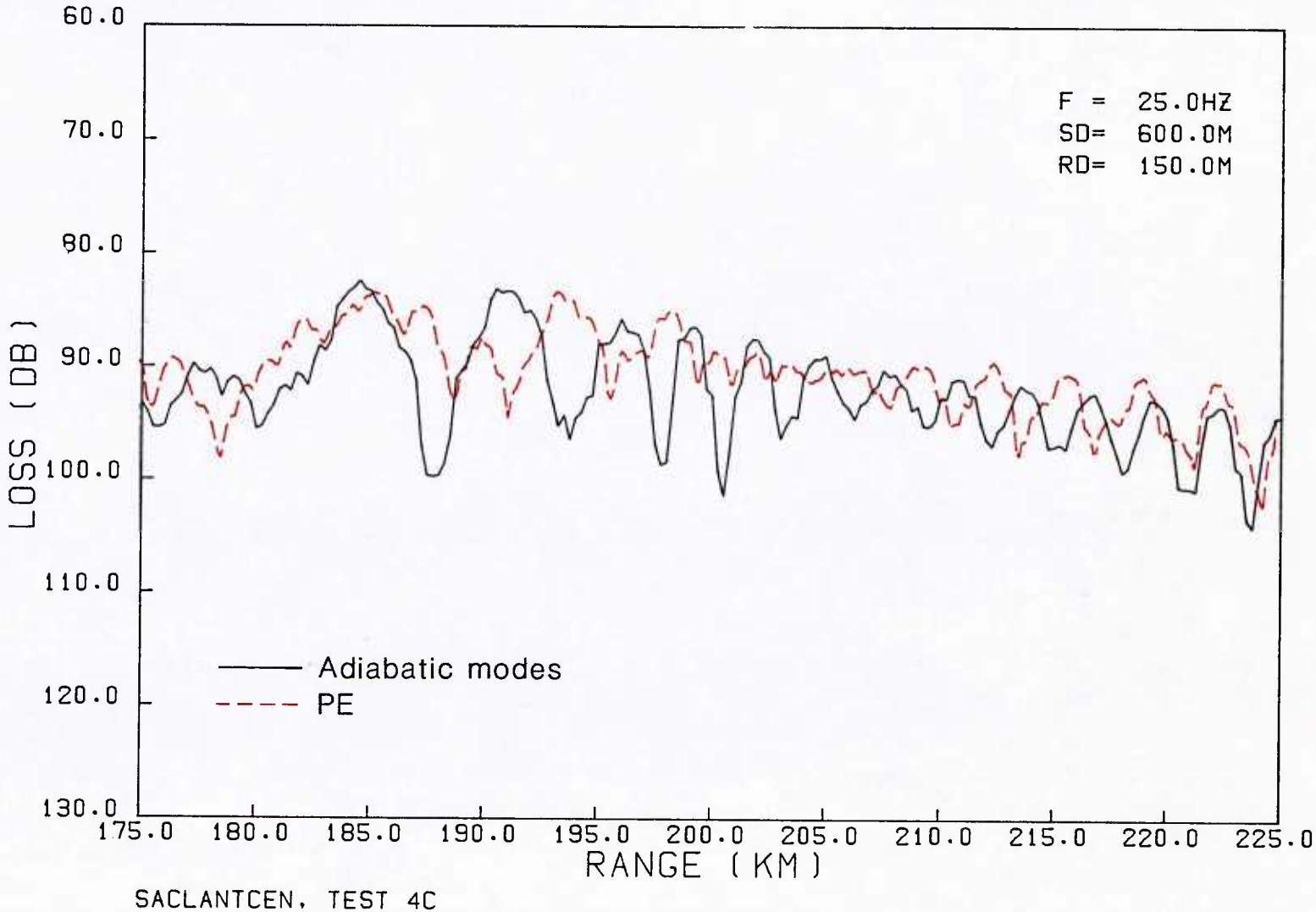


*FIG. 17 INTER-MODEL COMPARISON FOR CASE 4C*

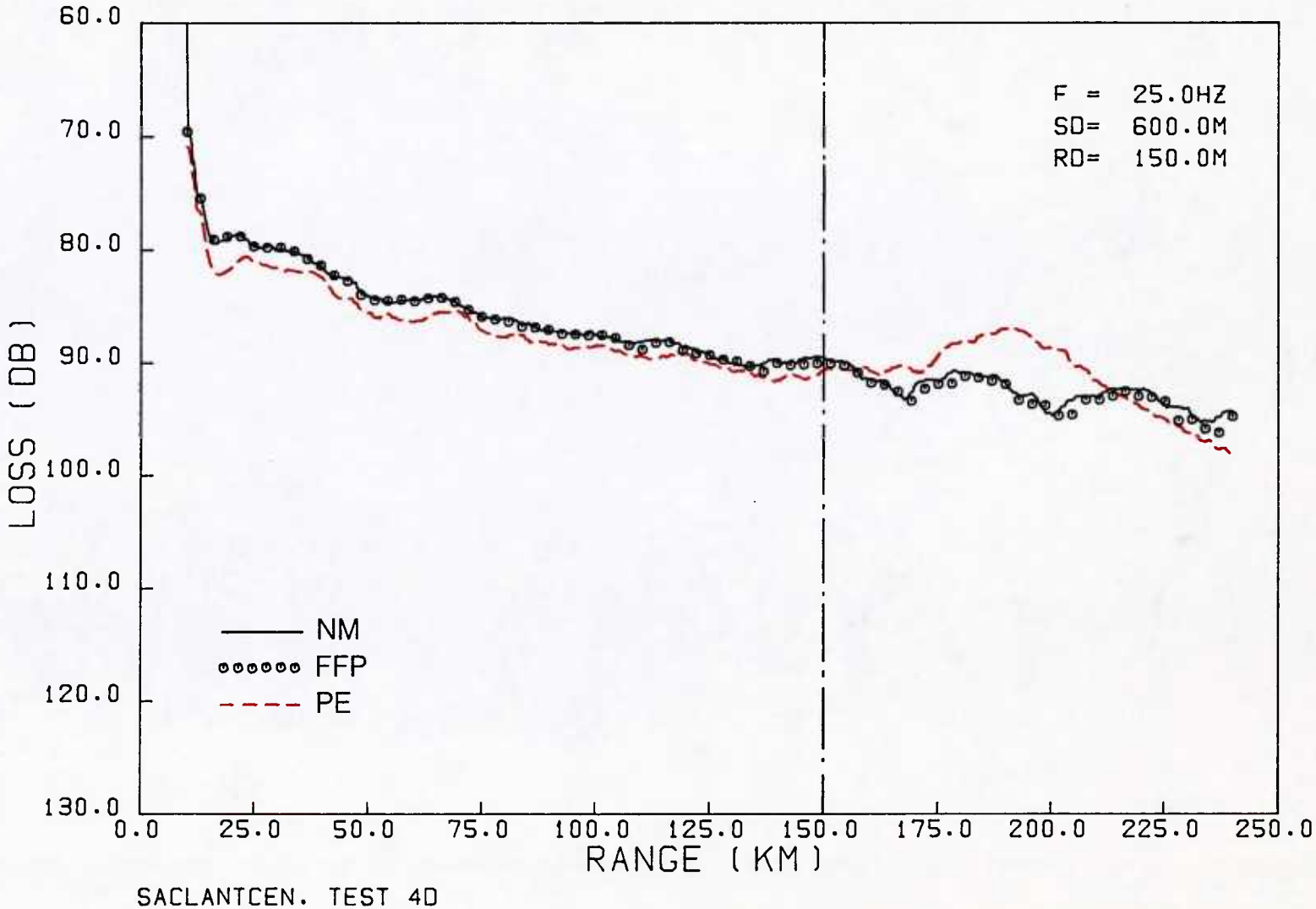


*FIG. 18 INTER-MODEL COMPARISON FOR CASE 4D*

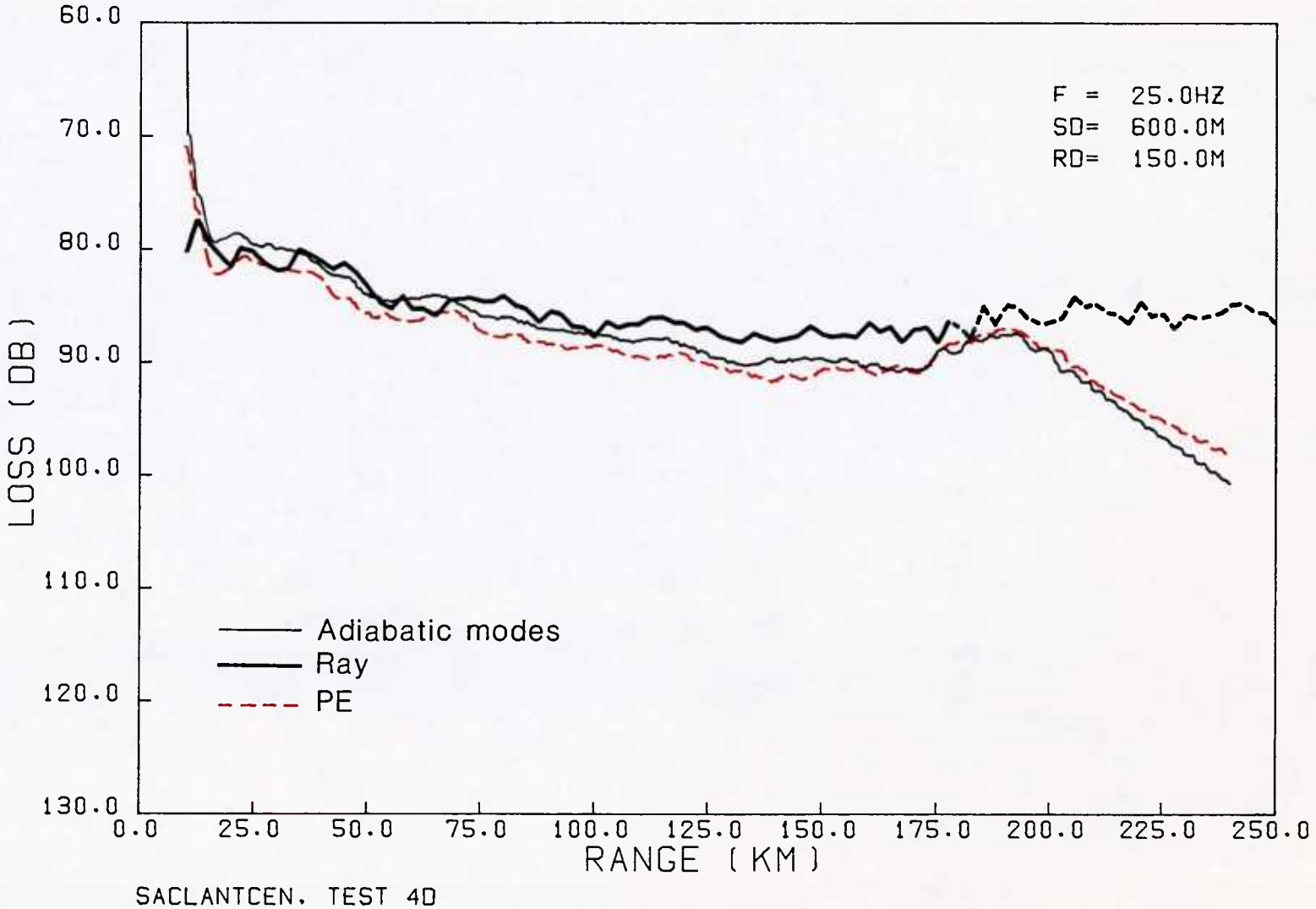


*FIG. 19 COMPARISON OF THREE RANGE-DEPENDENT MODEL RESULTS FOR CASE 4D*

# APPENDICES

# APPENDIX A

## MATHEMATICAL FOUNDATION OF ACOUSTIC MODELS

In this appendix we briefly present the mathematical foundations of the models used in the main body of this report. A more detailed description can be found in references A.1 to A.9. Appendix B describes the specific models used.

The starting point for all the models is the wave equation for a harmonic point source with time dependence exp(-iωt),

$$\nabla^2\phi(x,y,z) + \left[\frac{\omega}{c(x,y,z)}\right]^2 \phi(x,y,z) = -\delta(x-x_o)\delta(y-y_o)\delta(z-z_o) \qquad \text{(Eq. A.1)}$$

$$\psi = \phi\exp(-i\omega t) \qquad \text{(Eq. A.2)}$$

At any point (x,y,z) in the medium, the velocity potential $\phi$ satisfies Eq. A.1, where c(x,y,z) is the sound speed of the medium and $\delta$ is the Dirac delta function. The source is at the coordinate $(x_o,y_o,z_o)$, where z is the depth coordinate, which is taken to be positive in the downward direction from the ocean surface.

For the boundary condition at the ocean surface we take the density of air to be negligible compared with that of water; hence, the pressure must vanish at the ocean surface ("pressure-release surface"). At a boundary between two media such as the ocean and the ocean bottom, the balancing of forces at the interface require that physical quantities such as particle velocity and pressure be continuous across the boundary:

$$v_i = -\frac{\partial\phi}{\partial x_i} \; ; \quad x_i = x,y, \text{ or } z \qquad \text{(Eq. A.3)}$$

$$p = -i\omega\rho\phi \qquad \text{(Eq. A.4)}$$

If the ocean bottom is treated as an elastic medium that can support shear motions, there is the additional boundary condition that tangential stress must be continuous. Since the water column cannot support shear waves, this requires that the tangential stress in the ocean bottom vanishes at the interface.

The four widely used solution techniques for Eq. A.1 are schematically represented below in Fig. A.1.

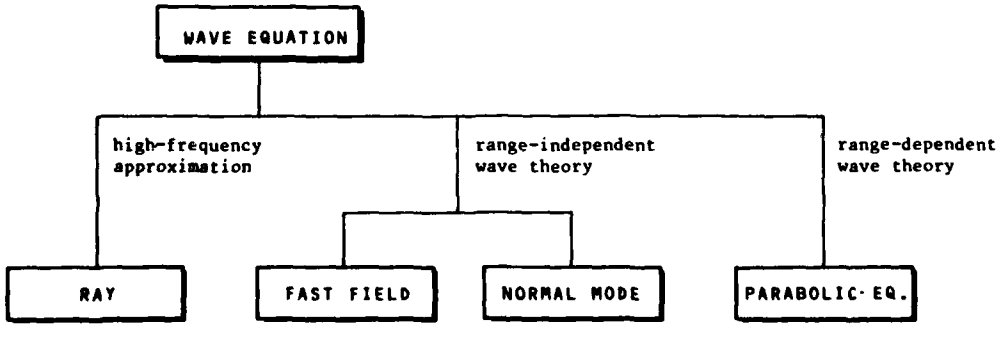


*FIG. A.1 TECHNIQUES FOR SOLVING THE WAVE EQUATION*

We now briefly describe the derivation of these solutions, starting with range-independent wave theory.

## A.1 Fast Field Solution

Here we are solving the wave equation for the case where the sound-speed profile is only a function of depth and the bottom is flat; this type of environment is often referred to as the horizontally stratified ocean. From Eq. A.1 we therefore have that $c(x,y,z)$ is simply $c(z)$. Because the environment is independent of "r", the horizontal coordinates $(x,y)$, one possible method of solving Eq. A.1 is to Fourier decompose the acoustic field into an infinite set of horizontal waves:

$$\phi(x,y,z) = \frac{1}{2\pi} \int d^2\vec{\eta}\; u(\vec{\eta},z)\; e^{i\vec{\eta}\cdot\vec{r}} \quad . \qquad \text{(Eq. A.5)}$$

Substituting Eq. A.5 into Eq. A.1 we obtain the equation for $\phi(\eta_x,\eta_y;z)$,

$$\frac{\partial^2 u(\eta_x,\eta_y;z)}{dz^2} + [k^2(z) - \eta^2]u(\eta_x,\eta_y;z) = -\frac{1}{2\pi}\,\delta(z - z_o), \qquad \text{(Eq. A.6)}$$

where $k(z) = \omega/c(z)$ and $\eta^2 = \eta_x^2 + \eta_y^2$, is the horizontal wavenumber of the individual plane waves.

*Using polar coordinates we can rewrite Eq. A.5 as*

$$\phi(r,z) = \frac{1}{2\pi} \int_o^{2\pi} d\theta \int_o^{\infty} \eta\; d\eta\; u(\eta,z)e^{i\eta r\cos\theta} \quad . \qquad \text{(Eq. A.7)}$$

We now integrate over the azimuthal angle to obtain

$$\phi(r,z) = \int_o^{\infty} \eta\; d\eta\; u(\eta,z)J_o(\eta r) \quad , \qquad \text{(Eq. A.8)}$$

where $J_o$ is the zero$^{th}$ order Bessel function. Using the relationship that

$$J_o(\eta r) = \frac{1}{2}\,[H_o^{(1)}(\eta r) + H_o^{(2)}(\eta r)] \quad ,$$

where the H's are Hankel functions and noting from Eq. A.6 that $u(\eta,z)$ is even in $\eta$, we can rewrite Eq. A.8 as

$$\phi(r,z) = \frac{1}{2}\int_{-\infty}^{\infty} \eta\; d\eta\; u(\eta,z)\; H_o^{(1)}(\eta r) \quad , \qquad \text{(Eq. A.9)}$$

where now the integration over $\eta$ is from $-\infty$ to $\infty$. For ranges greater than a few wavelengths from the source, the asymptotic form of the Hankel function can be used:

$$H_0^{(1)}(\eta r) \sim (2/\pi\eta r)^{\frac{1}{2}} \exp[i(\eta r - \pi/4)]$$

and, hence, Eq. A.9 can be expressed as

$$\phi(r,z) = \frac{e^{-i\pi/4}}{\sqrt{2\pi}} \cdot \frac{1}{\sqrt{r}} \int_{-\infty}^{\infty} d\eta \sqrt{\eta} u(\eta,z) e^{i\eta r} , \qquad \text{(Eq. A.10)}$$

where the factor $1/\sqrt{r}$ indicates cylindrical spreading.

Equation A.10 can be numerically integrated to obtain the acoustic field at the range r and depth z. In order to do this we must solve Eq. A.6 for many $\eta$'s to have a sufficient set of u's as a function of $\eta$ so that the integration over $\eta$ in Eq. A.10 can be performed. Given that u has has been obtained numerically as a function of $\eta$, the integration can be done using an FFT algorithm. This total procedure is called the Fast Field Program (FFP) <A.10, A.11>, although most of the numerical effort goes into solving Eq. A.6 for the many $\eta$'s. For computation we discretize Eq. A.10 by letting

$$\eta_m = \eta_o + m\Delta\eta; \; r_n = r_o + n\Delta r; \; (m,n) = 0,1,2\ldots,N-1 , \qquad \text{(Eq. A.11)}$$

with the additional relation

$$\Delta r \Delta\eta = \frac{2\pi}{N} \qquad \text{(Eq. A.12)}$$

and N is an integral power of two. Note that the discretization relations of Eq. A.11 restricts the solution to outgoing waves. Substituting Eq. A.11 into Eq. A.10 we obtain

$$\phi(r_n,z) = \Delta\eta \frac{e^{-i\pi/4}}{\sqrt{2\pi r}} e^{i\eta_o r_n} \sum_{M=0}^{N-1} X_m e^{i2\pi mn/N} , \qquad \text{(Eq. A.13)}$$

and hence the input to the FFT is

$$X_m = \sqrt{\eta_m}\, u(\eta_m,z) e^{imr_o\Delta\eta} . \qquad \text{(Eq. A.14)}$$

Equations A.13 and A.14 specify the numerical procedure to be employed in solving the wave equation using the FFP approach after Eq. A.6 has been solved numerically for the complete set of u's as a function of $\eta$. As mentioned above, the main effort in the FFP approach is the numerical integration of Eq. A.6 and not the final implementation of Eqs. A.13 and A.14, which is a simple FFT computation. Numerical procedures for integrating Eq. A.6 are given in references A.10 and A.11.

The advantages of the FFP are that it includes the "nearfield", and it can include shear propagation effects with no restrictions on the shear velocity relative to the water's compressional-wave velocity. Its disadvantages are that the procedure is not easily automated, only one source/receiver depth configuration can be done for each numerical solution (see Eqs. A.6, A.13 and A.14) and the sampling of the field in range is restricted by Eq. A.12.

## A.2 Normal-Mode Solution

The alternative to a direct numerical integration of Eq. A.6 is to expand u into a complete set of normal modes:

$$u(\eta_x,\eta_y;z) = \sum a_n(\eta_x,\eta_y)u_n(z), \qquad \text{(Eq. A.15)}$$

where the $u_n$'s are the solutions to the eigenvalue equation

$$\frac{d^2u_n(z)}{dz^2} + [k^2(z) - k_n^2]u_n(z) = 0 \qquad \text{(Eq. A.16)}$$

that satisfies the above-mentioned boundary conditions. In addition, we require the $u_n(z)$ be bounded as $z \to \infty$. The normal modes $u_n(z)$ form a complete orthonormal set that satisfies the relation

$$\int_0^\infty \rho(z)u_n(z)u_m(z)dz = \delta_{nm}, \qquad \text{(Eq. A.17)}$$

where the density $\rho(z)$ takes its appropriate value in each layer and $\delta_{nm}$ is the Kronecker-delta symbol. The spectrum of eigenvalues consists of a discrete part and a continuous part, the discrete eigenvalues occurring in the interval

$$\omega/c_2 < k_n < \max[\omega/c(z)], \qquad \text{(Eq. A.18)}$$

where $c_2$ is the highest speed of the system. In the present treatment we consider only the discrete eigenvalues, since in general the continuous spectrum makes a negligible contribution beyond the nearfield of the source (and requires an FFP-type calculation in any event).

We now substitute Eq. A.15 into Eq. A.6, multiply the resulting equation by $\rho(z)u_m(z)$, and integrate over z from 0 to $\infty$, giving:

$$a_n = \frac{1}{2\pi}\frac{\rho(z_o)u_n(z_o)}{\eta^2 - k_n^2}. \qquad \text{(Eq. A.19)}$$

Substituting Eqs. A.15 and A.19 back into Eq. A.5 we obtain an integral representation of the velocity potential,

$$\phi(x,y,z) = \frac{\rho(z_o)}{(2\pi)^2} \int_{-\infty}^{\infty} d\eta_x \int_{-\infty}^{\infty} d\eta_y \sum_n \frac{u_n(z_o)u_n(z)}{\eta^2 - k_n^2}$$

$$x \exp[i(\eta_x x + \eta_y y)] \ . \qquad \text{(Eq. A.20)}$$

We evaluate the above integral by choosing a path about the poles so as to lead to an outgoing wave from the source point r = 0. Each integral in Eq. A.20 is proportional to the two-dimensional plane-wave representation of the zero-order Hankel function of the first kind <A.12>, and therefore $\phi(x,y,z)$ can be expressed as:

$$\phi(r,z) = \frac{i}{4} \rho(z_o) \sum_n u_n(z_o)u_n(z)H_o^{(1)}(k_n r) \ . \qquad \text{(Eq. A.21)}$$

The asymptotic form of the Hankel function can then be used to obtain

$$\phi(r,z) = \frac{i\rho(z_o)}{(8\pi r)^{\frac{1}{2}}} e^{-i\pi/4} \sum_n \frac{u_n(z_o)u_n(z)}{k_n^{\frac{1}{2}}} e^{ik_n r} \ . \qquad \text{(Eq. A.22)}$$

In addition to the decay of the field due to cylindrical spreading, other loss mechanisms such as volume attenuation in the water column and bottom are included in Eq. A.22 because the eigenvalues, $k_n$, have positive imaginary parts <A.13>, thereby resulting in an exponential attenuation of each normal-mode term. Equation A.22 gives us the important result that the field at a depth z is proportional to a sum of the products of normal modes evaluated at the source and the receiver depth. The normal modes are the "natural vibrations" of the system and if a point source is located at the null of a particular normal mode, that mode will not be excited. Similarly, if a point receiver is placed at the null of a particular mode, that mode contribution to the total field will not be sensed.

In analogy to the FFP procedure, the main numerical effort for the normal-mode procedure is the solution of the eigenvalue problem defined by Eq. A.16 and the boundary conditions. There are many techniques to solve this equation <A.14, A.15> but they are mainly applicable to low-frequency or shallow-water propagation, where there is only a small number of modes <A.16>. However, there are also techniques to handle deep-water high-frequency propagation using normal modes <A.17>.

The advantages of the normal-mode procedure are, first, that once Eq. A.16 is solved we have the solution for all source/receiver configurations, and, second, that the whole solution procedure can be highly automated. In addition, the normal-mode procedure can be easily extended to slightly range-dependent environments using the adiabatic approximation where mode coupling is neglected <A.18 to A.23>; numerical methods for including mode-coupling effects are present areas of research <A.24 to A.27>. The disadvantages of the normal-mode solution are that conventional procedures do not include nearfield effects (the exception is Stickler's work <A.28>, but even there the nearfield is evaluated with a procedure similar to the FFP approach) and there are restrictions on how one can treat shear propagation in the bottom.

## A.3 The Relation Between Normal-Mode (NM) and Fast-Field (FFP) Solutions

Both FFP and normal modes are solutions of Eqs. A.5 and A.6. The difference between the two is that the normal-mode method restricts the integration to horizontal wavenumber ($\eta$ is a continuously varying horizontal wavenumber, whereas $k_n$ are the discrete horizontal wavenumbers) in the interval corresponding to the discrete portion of the spectrum defined by Ineq. A.18. From Eq. A.20, we see that the integrand has poles at $\eta = k_n$. Hence, the function u in Eq. A.10 and $X_m$ of Eqs. A.13 and A.14 should have poles at the same locations.

Figure A.2 shows a plot of the FFP integrand for case 2A. The horizontal axis is the wavenumber ($\eta$) and the vertical axis is a normalized absolute value of the integrand amplitude. The vertical dashed line separates the discrete spectrum (defined by Ineq. A.18) and the continuous spectrum. A blowup of the discrete spectrum is shown in Fig. A.3. In this particular case there are eleven modes. The plot shown in Fig. A.3 is an FFP integrand and the asterisks on the plot are the locations and the amplitudes of the modes from a NM calculation. We see that the eigenvalues as calculated from the NM program (Table A.1) coincide precisely with the peaks (poles), and also that the NM amplitudes correspond to the amplitudes of the peaks. (It turns out that this one-to-one correspondence in the amplitudes is because there is virtually no loss in this problem. Otherwise, the correspondence would not be as precise because loss shows up in the FFP calculation as widths in the peaks; nevertheless, for realistic losses the location of the poles would be the same.)

TABLE A.1

MODAL EIGENVALUES FROM SNAP

| Mode no. | Wavenumber ($m^{-1}$) |
|---|---|
| 1 | 0.10423 |
| 2 | 0.10386 |
| 3 | 0.10356 |
| 4 | 0.10328 |
| 5 | 0.10297 |
| 6 | 0.10261 |
| 7 | 0.10221 |
| 8 | 0.10182 |
| 9 | 0.10142 |
| 10 | 0.10102 |
| 11 | 0.10064 |

Figure A.4 displays the amplitudes of the eleven modes plotted as a function of depth. The dashed line indicates the source/receiver position. Notice the high excitation of the second mode and the low excitation of the third, sixth, and ninth modes, and notice the one-to-one correspondence with the FFP integrand shown in Fig. A.3.

This particular example shows the consistency between FFP and NM calculations. In the next section we show the results on transmission loss when discrete and discrete-plus-continuous spectra are included and we compare them with PE calculations.

## A.4 Parabolic Equation

If the environment varies both in range and depth, the wave equation cannot be separated and therefore direct numerical integration is required. At present there are no practical methods to perform this direct integration of the three-dimensional wave equation, which is a boundary-value problem. An alternative approach is to derive an approximate wave equation that lends itself to practical numerical solution. We now outline the derivation of such an approximation, the Parabolic Equation (PE) <A.29>.

The velocity potential is decomposed as follows:

$$\phi = \psi(r, z) \cdot S(r), \qquad \text{(Eq. A.23)}$$

and we substitute $\phi$ into Eq. A.1 in a source-free region:

$$\psi \cdot \left[\frac{\partial^2 S}{\partial r^2} + \frac{1}{r}\frac{\partial S}{\partial r}\right] + S \cdot \left[\frac{\partial^2 \psi}{\partial r^2} + \frac{\partial^2 \psi}{\partial z^2} + \left(\frac{1}{r} + \frac{2}{S}\frac{\partial S}{\partial r}\right) \cdot \frac{\partial \psi}{\partial r} + k_o^2 n^2 \psi\right] = 0. \qquad \text{(Eq. A.24)}$$

That is, we will eventually end up with an equation that allows a "marching-in-range" solution and we will have to initialize the solution in some way (see below). We use the notation that

$$k^2 = k_o^2 n^2 , \qquad \text{(Eq. A.25)}$$

where n is an "index of refraction" equal to $c_o/c$, where $c_o$ is a reference speed.

Equation A.24 may be separated into two differential equations by setting the terms in the first bracket equal to $-Sk_o^2$ and the terms in the second bracket equal to $\psi k_o^2$, where $k_o^2$ is the separation constant. The functions $S(r)$ and $\psi(r,z)$ then have to satisfy the following two equations:

$$\frac{\partial^2 S}{\partial r^2} + \frac{1}{r}\frac{\partial S}{\partial r} + k_o^2 S = 0 \qquad \text{(Eq. A.26)}$$

$$\frac{\partial^2 \psi}{\partial r^2} + \frac{\partial^2 \psi}{\partial z^2} + \left(\frac{1}{r} + \frac{2}{S}\frac{\partial S}{\partial r}\right) \cdot \frac{\partial \psi}{\partial r} + k_o^2 n^2 \psi - k_o^2 \psi = 0. \qquad \text{(Eq. A.27)}$$

The solution of Eq. A.26 is the zero$^{th}$ order Hankel function, $H_o^{(1)}(k_o r)$, whose asymptotic form has been given in Sect. A.1. Substituting the asymptotic form of the Hankel function into Eq. A.27 and making the paraxial approximation

$$\frac{\partial^2 \psi}{\partial r^2} << 2k_o \frac{\partial \psi}{\partial r} , \qquad \text{(Eq. A.28)}$$

we obtain

$$\frac{\partial^2\psi}{\partial z^2} + 2ik_o \frac{\partial\psi}{\partial r} + k_o^2(n^2 - 1)\,\psi = 0, \qquad \text{(Eq. A.29)}$$

which is the parabolic wave equation.

The paraxial approximation is a narrow-angle approximation. It implies that the rapid range dependence of Eq. A.23 is included in S(r), while $\psi$ is a function varying more slowly in r. An approximation to solving Eq. A.29 is to assume that n is not a function of the spatial variables but is a constant. It is shown elsewhere <A.29, A.30> that the error introduced can be made arbitrarily small by using numerical methods. With n a constant, we can Fourier transform $\psi$ with respect to z,

$$\psi(r,s) = \frac{1}{2\pi} \int_{-\infty}^{\infty} \psi(r,z)e^{-isz}dz, \qquad \text{(Eq. A.30)}$$

which together with Eq. A.29 gives

$$-s^2\psi + 2ik_o \frac{\partial\psi}{\partial r} + k_o^2(n^2 - 1)\,\psi = 0. \qquad \text{(Eq. A.31)}$$

Equation A.31 is a first-order differential equation with constant coefficients and has the solution

$$\psi(r,s) = \psi(r_o,s) \cdot e^{-\frac{k_o^2(n^2 - 1) - s^2}{2ik_o}(r - r_o)} \qquad \text{(Eq. A.32)}$$

where the initial condition at $r_o$ must be specified. The field as a function of depth is the inverse transform of Eq. A.30

$$\psi(r,z) = \int_{-\infty}^{\infty} \psi(r_o,s) \cdot e^{\frac{iko}{2}(n^2 - 1)\Delta r} \; e^{-\frac{i\Delta r}{2k_o}s^2} \cdot e^{isz}ds \qquad \text{(Eq. A.33)}$$

where $\Delta r = r - r_o$.

By introducing the symbol $\mathcal{F}$ for the fourier transform from the z-domain and $\mathcal{F}^{-1}$ as the inverse transform, Eq. A.33 may be written as

$$\psi(r + \Delta r,z) = e^{\frac{ik_o}{2}(n^2 - 1)\Delta r} \cdot \mathcal{F}^{-1}\left\{ e^{-\frac{i\Delta r}{2k_o}s^2} \cdot \mathcal{F}\{\psi(r,z)\}\right\}. \qquad \text{(Eq. A.34)}$$

Equation A.34 is the so-called "split-step" marching solution of the parabolic equation. The fourier transforms are performed using an FFT. It is the solution for n constant, but the error introduced when n (profile and bathymetry) varies with range and depth can be made arbitrarily small by increasing the transform size and decreasing the range-step size <A.29, A.30>.

The parabolic equation is not a boundary-value equation as we have numerically formulated it above. We can include the surface boundary condition by taking an anti-symmetric FFT about the sea surface ($z = 0$). In practice this is performed by taking sine transforms. The boundary conditions in the bottom are simulated by including the discontinuity in velocity in the sound-speed profile. There are methods to also include the density discontinuity <A.29>. The radiation condition as z goes to infinity is simulated by requiring the field to exponentially tail off for large values of z beyond which there would not be any significant acoustic interaction.

As mentioned above, the PE method requires an initial starting solution. Two methods have been used for describing a point source. The first method is to initialize the field with a set on normal modes descriptive of the point source in the starting environment. This would not include the continuous portion of the spectrum (see Sect. A.3), but for long-distance propagation this approximation is adequate. A second approach has proved to be simpler and as effective. The point source is approximated by two gaussians that are anti-symmetric about the sea surface, thereby automatically including the pressure-release boundary condition at the surface. It is this last technique that has been used in this report and we have found that not only is this a good approximation, but we have also shown that by using this technique part of the continuous spectrum is included.

In Sect. A.3 we compared FFP and NM, using test case 2A as an example. We now look at transmission loss from the point of view of discrete, discrete-plus-continuous, and PE, which does not obviously distinguish between regions in the spectrum. Figure A.5 shows test case 2A plotted from 0 to 6 km. Note that the PE tracks the FFP results in the nearfield indicating that at least part of the continuous portion of the spectrum is included in the PE calculation. Figure A.6 for the full range of 20 km, shows how the three model results converge in the farfield; recall that the NM calculation does not include the full nearfield contribution. This particular example clearly illustrates the consistency and inter-relationship between the three models.

The advantages of the PE are that it handles a range-dependent environment and gives the acoustic field in the entire water column without additional computational effort. Its disadvantages are that the procedure is not easily automated, and it is practical only for low-frequency propagation since computation times increase with frequency squared. Moreover, there is no straightforward way of handling shear propagation in the bottom.

## A.5 Ray theory

This report is concerned mainly with wave theory; nevertheless, for completeness, we include a brief description of ray theory. In this case

we assume a solution of Eq. A.1 (with right-hand side equal to zero) as

$$\phi = \psi(x,y,z) \cdot e^{iS(x,y,z)}. \qquad \text{(Eq. A.35)}$$

$S(x,y,z)$ is a phase function that includes rapid variations as a function of range, and $\psi(x,y,z)$ is a more slowly varying envelope function in which geometrical spreading and loss mechanisms are included (in the PE, S contains the cylindrical spreading factor). Substituting Eq. A.35 into the wave equation and separating real and imaginary parts, we obtain

$$\frac{1}{\psi} \nabla^2\psi - (\nabla S)^2 + k^2 = 0, \quad 2(\nabla\psi \cdot \nabla S) + \psi\nabla^2 S = 0. \qquad \text{(Eq. A.36)}$$

We now make the geometrical-acoustics approximation

$$\frac{1}{\psi} \nabla^2\psi << k^2, \qquad \text{(Eq. A.37)}$$

that is, the amplitude of the phase function varies slowly in range with respect to wavelength. Substituting Eq. A.37 in Eq. A.36 gives the eikonal equation,

$$(\nabla S)^2 = k^2. \qquad \text{(Eq. A.38)}$$

The trajectory of the rays is perpendicular to the surfaces of constant phase (wavefronts), S, and is expressed by

$$\frac{d}{d\ell} \left\{ k \frac{d\vec{X}}{d\ell} \right\} = \nabla k, \qquad \text{(Eq. A.39)}$$

where $\ell$ is the arc length along a ray and X is the coordinate. It can be shown that the direction of the average energy flow is along these trajectories and the amplitude of the field at any point can be obtained from the density of these rays; formally, having solved for S, the amplitude is obtained from solving the second part of Eq. A.36. We also mention here that corrected ray theory assumes that $\psi$ is a function of frequency and an expansion in powers of inverse frequency is made, the leading term being the infinite-frequency solution with the additional terms being corrections from the infinite-frequency solution.

The advantages of ray theory methods are that the computations are rapid and that ray traces give a very physical picture of the acoustic paths. The disadvantage is that ray-theory is an infinite-frequency approximation and therefore does not include diffraction and other wave effects. This shortcoming also prevents ray theory from adequately describing significant bottom interaction and low-frequency ducted propagation.

## REFERENCES


A.1 OFFICER, C.B. Introduction to the Theory of Sound Transmission. New York, McGraw-Hill, 1958.

A.2 TOLSTOY, I. and CLAY, C.S. Ocean Acoustics: Theory and Experiment in Underwater Sound. New York, McGraw-Hill, 1966.

A.3 TUCKER, D.G. and GAZEY, B.K. Applied Underwater Acoustics. Oxford, Pergamon, 1966.

A.4 TOLSTOY, I. Wave Propagation. New York, McGraw-Hill, 1973.

A.5 URICK, R.J. Principles of Underwater Sound. New York, McGraw-Hill, 1975.

A.6 CLAY, C.S. and MEDWIN, H. Acoustical Oceanography. New York, Wiley, 1977.

A.7 KELLER, J.B. and PAPADAKIS, J.S. eds. Wave Propagation and Underwater Acoustics. Berlin, Springer-Verlag, 1977.

A.8 DE SANTO, J.A. ed. Ocean Acoustics. Berlin, Springer-Verlag, 1979.

A.9 BREKHOVSKIKH, L.M. Waves in Layered Media. New York, Academic, 1980.

A.10 KUTSCHALE, H.W. Rapid computation by wave theory of propagation loss in the Arctic Ocean, Rpt CU-8-73. Palisades, N.Y., Columbia University, 1973

A.11 DINAPOLI, F.R. and DEAVENPORT, R.L. Theoretical and numerical Green's function field solution in plane multilayered medium. Journal Acoustical Society America 67, 1980: 92-105.

A.12 MORSE, P.M. and FESHBACH, H. Methods of Theoretical Physics. New York, McGraw-Hill, 1953, p. 823.

A.13 INGENITO, F., FERRIS, R., KUPERMAN, W.A. and WOLF, S.N. Shallow-water acoustics, summary report (first phase), Rpt. 8179. Washington, D.C., US Naval Research Laboratory, 1978.

A.14 SPOFFORD, C.W. A synopsis of the AESD workshop on acoustic-propagation modelling by non-ray-tracing techniques, Rpt. TN-73-05. Washington, D.C., Office of Naval Research, 1973.

A.15 JENSEN, F.B. and FERLA, M.C. SNAP: the SACLANTCEN normal-mode acoustic propagation model, SACLANTCEN SM-121. La Spezia, Italy, SACLANT ASW Research Centre, 1979. [AD A 067 256]

A.16 JENSEN, F.B. and KUPERMAN, W.A. Environmental acoustic modelling at SACLANTCEN, SACLANTCEN SR-34. La Spezia, Italy, SACLANT ASW Research Centre, 1979. [AD A 081 853]

A.17 FERLA, M.C., JENSEN, F.B. and KUPERMAN, W.A. High-frequency normal-mode calculations in deep water. Journal Acoustical Society America (to be published).

A.18 PIERCE, A.D. Extension of the method of normal modes to sound propagation in an almost stratified medium. Journal Acoustical Society America 37, 1965: 19-27.

A.19 MILDER, D.M. Ray and wave invariants for SOFAR channel propagation. Journal Acoustical Society America 46, 1969: 1259-1263.

A.20 WILLIAMS, A.O. Normal-mode methods in propagation of underwater sound. In: STEPHENS, R.W.B. ed., Underwater Acoustics. London, Wiley, 1970: 23-56.

A.21 NAGL, A., ÜBERALL, H., HAUG, A.J. and ZARUR, G.L. Adiabatic mode theory of underwater sound propagation in range-dependent environment. Journal Acoustical Society America 63, 1978: 739-749.

A.22 RUTHERFORD, S.R. and HAWKER, K.E. An examination of the influence of range dependence of the ocean bottom on the adiabatic approximation. Journal Acoustical Society America 66, 1979: 1145-1151.

A.23 RUTHERFORD, S.R. An examination of multipath processes in a range-dependent ocean environment winthin the context of adiabatic mode theory. Journal Acoustical Society America 66, 1979: 1482-1486.

A.24 CHWIEROTH, F.S., NAGL, A., ÜBERALL, H., GRAVES, R.D. and ZARUR, G.L. Mode coupling in a sound channel with range-dependent parabolic velocity profile. Journal Acoustical Society America 64, 1978: 1105-1112.

A.25 THOMPSON, I.J. Mixing of normal modes in a range-dependent model ocean. Journal Acoustical Society America 69, 1981: 1280-1289.

A.26 MCDANIEL, S.T. Comparison of coupled-mode theory with the small-waveheight approximation for sea-surface scattering. Journal Acoustical Society America 70, 1981: 535-540.

A.27 RUTHERFORD, S.R. and HAWKER, K.E. Consistent coupled mode theory of sound propagation for a class of nonseparable problems. Journal Acoustical Society America 70, 1981: 554-564.

A.28 STICKLER, D.C. Normal-mode program with both the discrete and branch line contributions. Journal Acoustical Society America 57, 1975: 856-861.

A.29 TAPPERT, F.D. The parabolic approximation method. In: KELLER, J.B. and PAPADAKIS, J.S. eds., Wave Propagation and Underwater Acoustics. Berlin, Springer-Verlag, 1977: 224-287.

A.30 JENSEN, F.B. and KROL, H.R. The use of the parabolic equation method in sound-propagation modelling, SACLANTCEN SM-72. La Spezia, Italy, SACLANT ASW Research Centre, 1975.

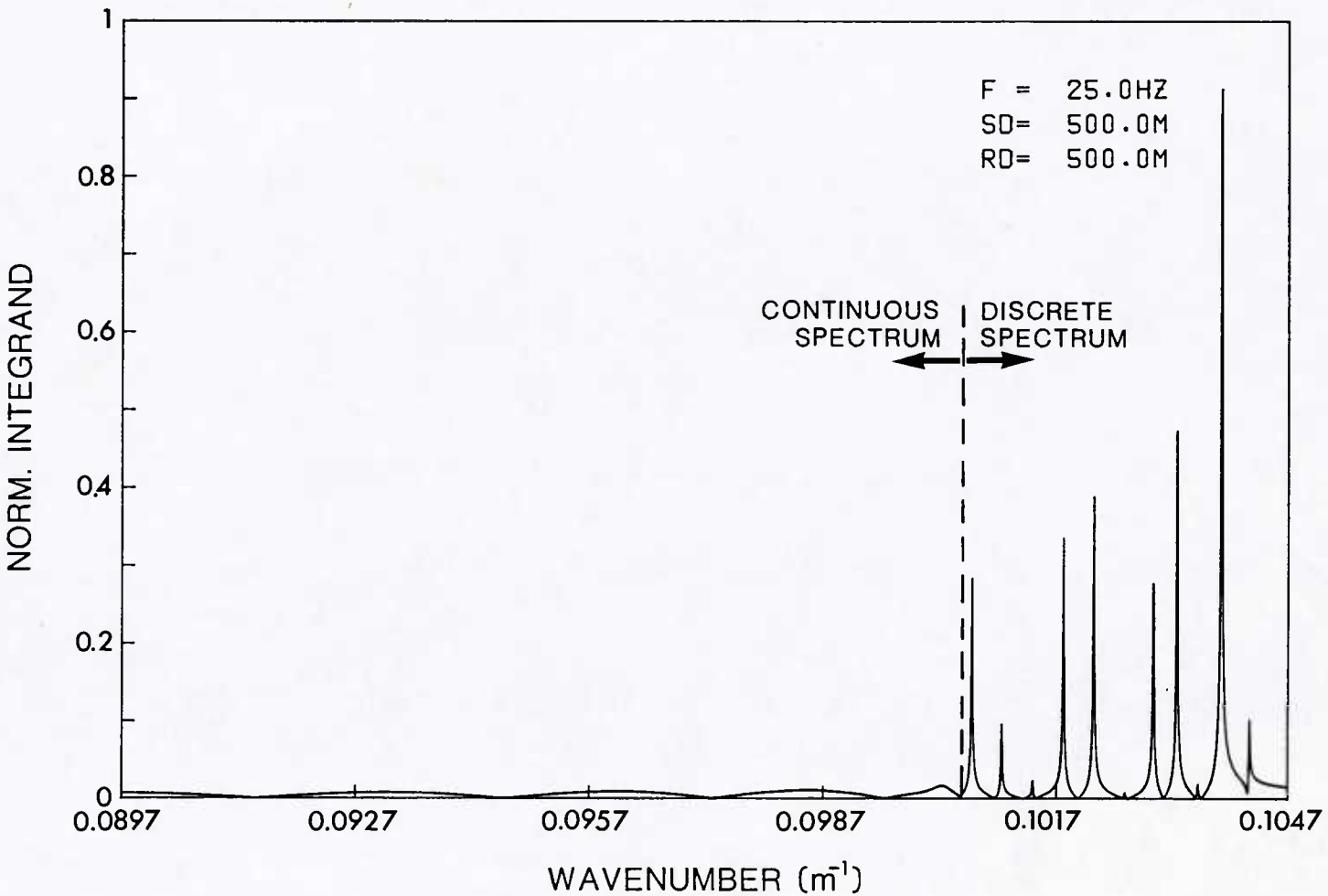


*FIG. A.2 FFP INTEGRAND PLOT FOR CASE 2A (full spectrum).*

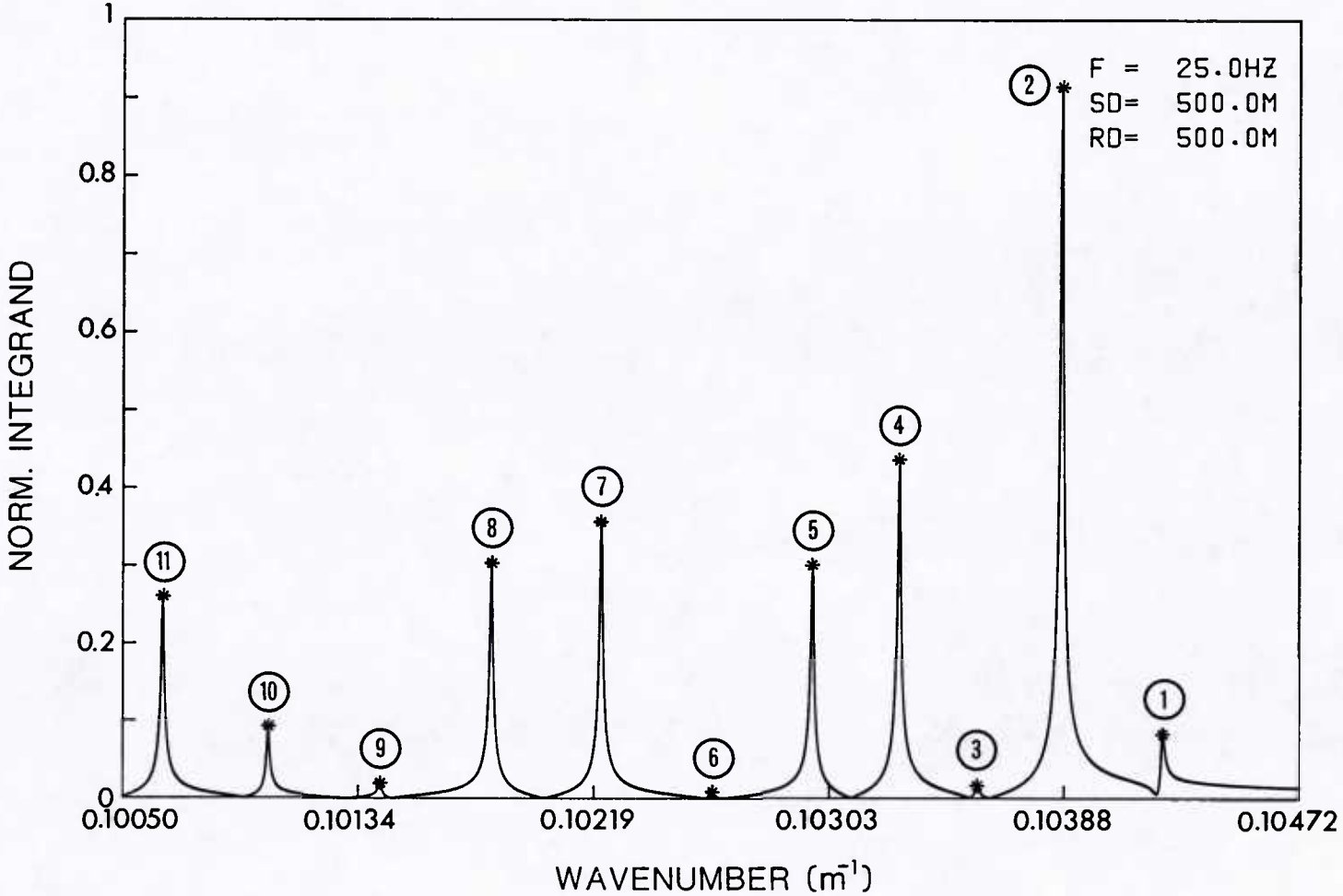


*FIG. A.3 FFP INTEGRAND PLOT FOR CASE 2A (discrete spectrum).*

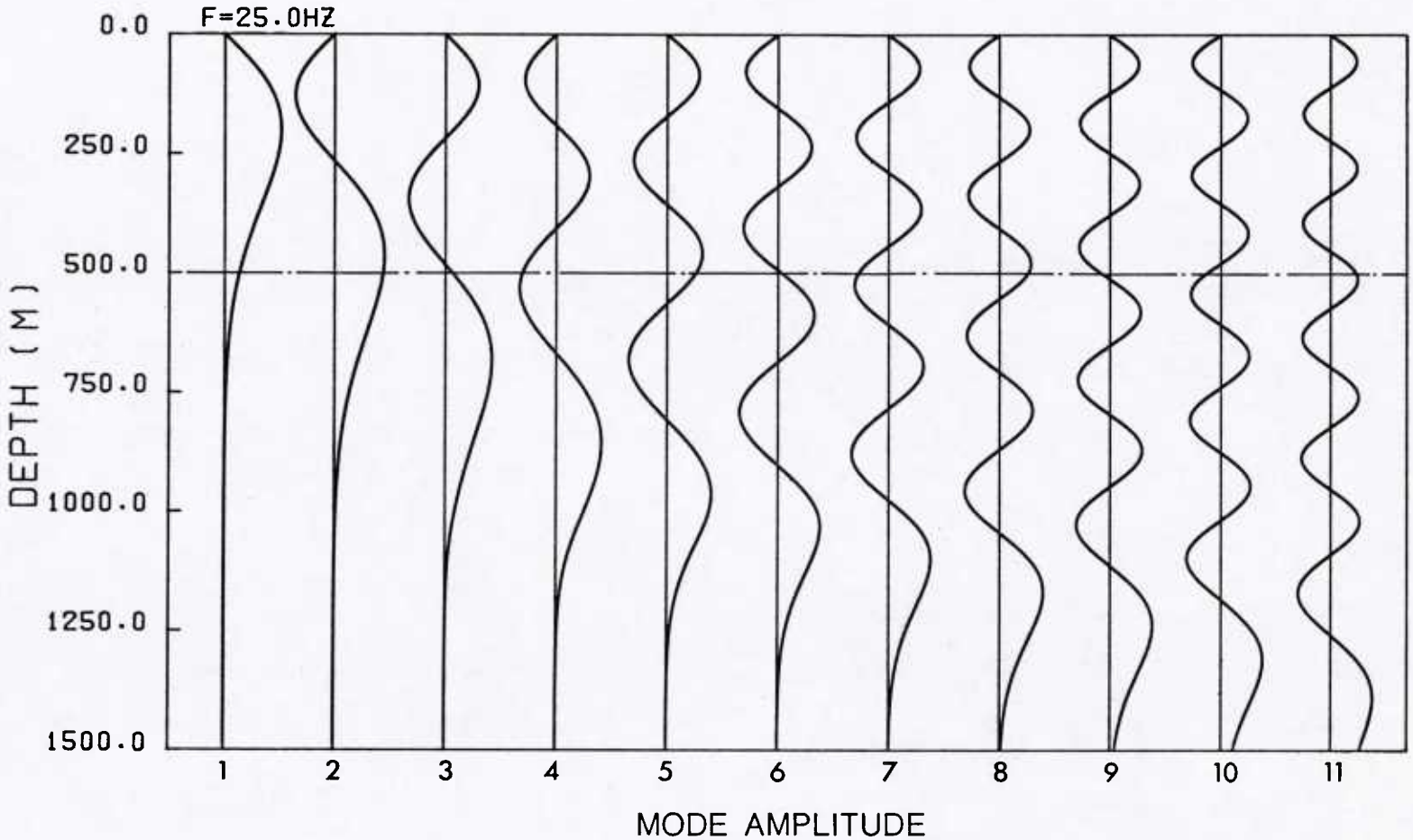


*FIG. A.4 MODE-AMPLITUDE FUNCTIONS FOR CASE 2A*

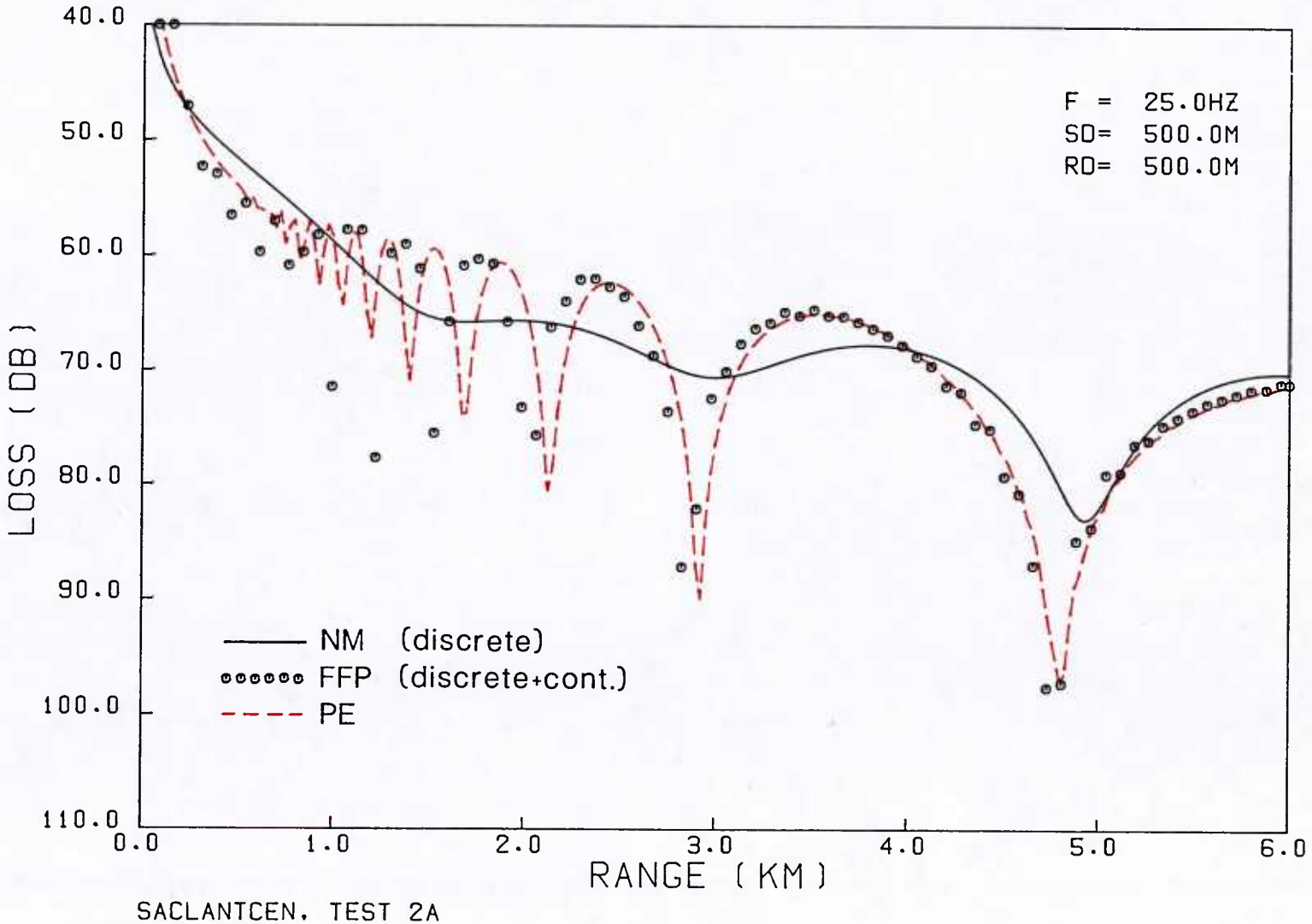


*FIG. A.5 INTER-MODEL COMPARISON FOR CASE 2A (near field)*

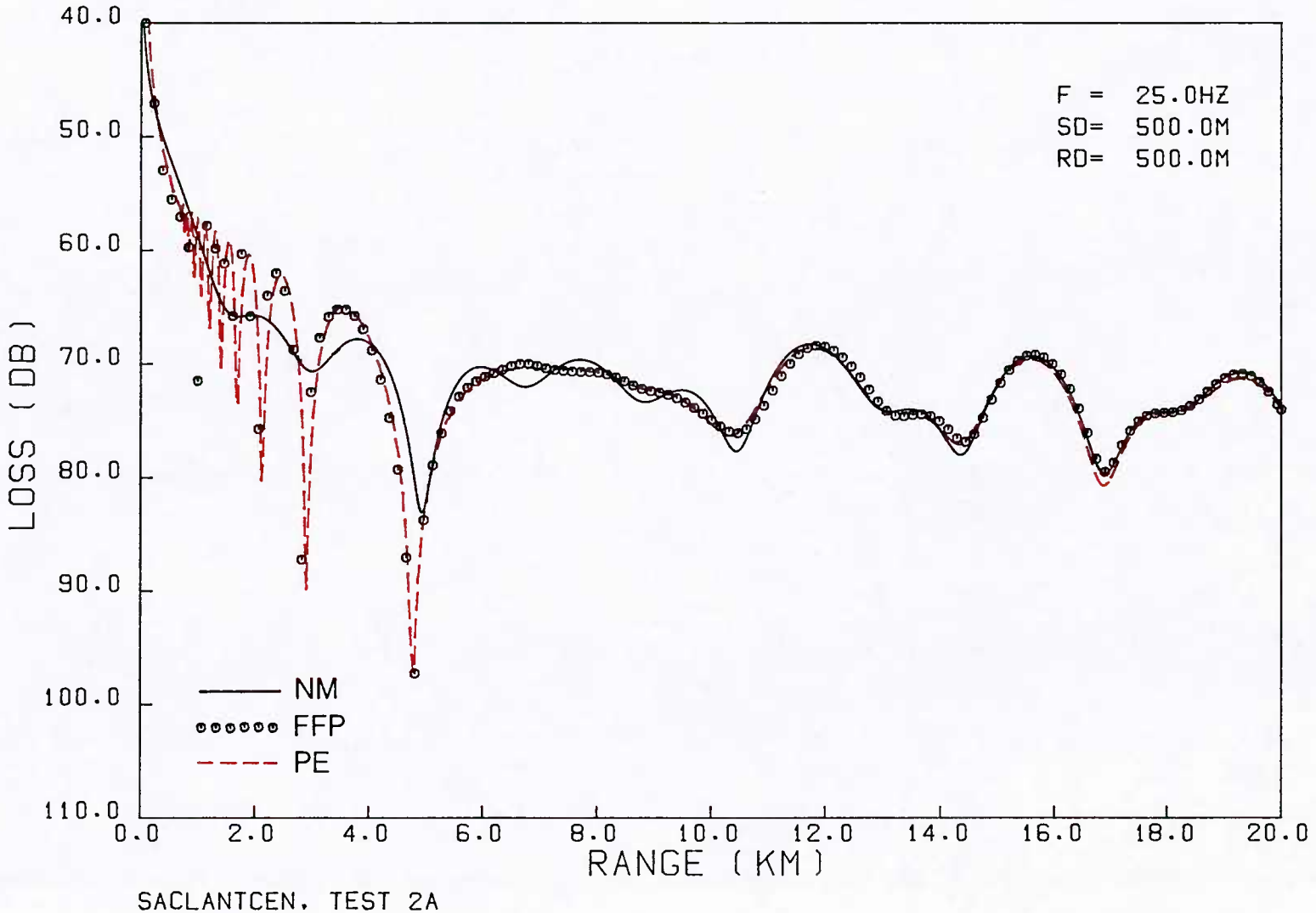


*FIG. A.6 INTER-MODEL COMPARISON FOR CASE 2A (far field)*

# APPENDIX B

# DESCRIPTION OF THE FOUR COMPUTER MODELS

## B.1 The FFP Model

The FFP model <B.1, B.2> is a complete numerical solution of the range-independent wave equation and hence includes the continuous part of the spectrum and the nearfield (distances greater than a wavelength). The model used in this study was developed at Columbia University <B.2>. It includes propagation of both compressional and shear waves and is therefore also suitable for seismic studies. In the original version, the depth-dependent part of the wave equation was solved using the Thompson-Haskell matrix method, where the water column is divided into isovelocity layers. An updated version <B.3> allows constant gradient in $k^2$ (equivalent to $1/c^2$ constant gradient) and therefore employs Airy functions in the Thompson-Haskell matrices instead of trigonometric functions. The inputs are the same as those of the normal-mode model (SNAP). There are two possible outputs. One output is the "integrand" plot, which is essentially a plot of energy versus wavenumber and therefore has maxima corresponding to the normal-mode eigenvalues in the discrete part of the spectrum; the maxima in the continuous portion of the spectrum correspond to the so-called "virtual modes". The second output is loss versus range. It should be noted, however, that the present program requires a complete new run for a change of source or receiver depth; hence, loss contours as functions of range and depth are not practical, as compared with normal-mode or PE methods.

## B.2 The SNAP Model

The SNAP Model <B.4> is a normal-mode model based on a program originally developed at the US Naval Research Laboratory <B.5, B.6>; this program solves the eigenvalue problem by direct numerical integration of the depth dependent equation. Computation time for some of the key subroutines has been reduced and the program has been restructured to run interactively on a UNIVAC EXEC-8 system. The model allows for slight range dependence by employing the adiabatic approximation. SNAP was originally designed for a shallow-water environment but there is now a version that handles high-frequency deep-water situations.

Environmental inputs are:

- arbitrary sound speed profile as function of depth (multiple profiles for range-dependent adiabatic computations) in the water column,
- density, attenuation, and compressional-velocity profile of sediment layer,
- density, shear velocity, compressional velocity, shear attenuation, and compressional attenuation of the basement.

At present, the output options are:

- loss vs range,
- loss vs depth,
- depth-averaged loss vs range,
- depth-averaged loss vs frequency,
- contoured loss vs frequency and range,
- contoured depth-averaged loss vs frequency and range,
- modal group velocity vs frequency,
- modal phase velocity vs frequency,
- mode function vs depth,
- phase of field vs depth,
- intensity of field vs arrival angle,
- sound speed vs depth.

The SNAP model has been subjected to extensive inter-model comparisons <B.7> as well as a thorough testing against experimental data <B.8, B.9>.

## B.3 The PAREQ Model

PAREQ <B.10, B.11> is a parabolic equation model; the computer program used in this study is a modified version of the one developed by the Acoustic Environmental Support Detachment (AESD) of the Office of Naval Research <B.12>. This model not only handles a variable sound-speed profile in depth and range but also allows the bottom depth and bottom structure to vary in range. The bottom is characterized by a compressional-velocity profile, density (the density discontinuity is smoothed using a hyberbolic tangent function as suggested in <B.10>) and attenuation, which is included by using a complex sound speed. The second layer of the bottom has constant acoustic properties. There are two options for the initial field: gaussian source or normal modes. The PAREQ model is not only resident on a UNIVAC 1100/60 but also runs on an HP 21MX computer. The model has recently been used to study mode conversion and mode cut-off phenomena in range-dependent environments <B.13>.

## B.4 The GRASS Model

GRASS <B.14> is a range-dependent ray-trace program originally developed at the US Naval Research Laboratory for a CDC 3800 computer. This version runs on a UNIVAC system; the only significant difference between the model used in this study and the original is that the input procedure has been simplified.

## REFERENCES


B.1 DINAPOLI, F.R. Fast field program for multilayered media, Rpt. 4103. New London, Conn., US Naval Underwater Systems Center, 1971.

B.2 KUTSCHALE, H.W. Rapid computation by wave theory of propagation loss in the Arctic Ocean, Rpt. CU-8-73. Palisades, N.Y., Columbia University, 1973.

B.3 KUTSCHALE, H.W. Unpublished communication.

B.4 JENSEN, F.B. and FERLA, M.C. SNAP: the SACLANTCEN normal-mode acoustic propagation model, SACLANTCEN SM-121. La Spezia, Italy, SACLANT ASW Research Centre, 1979. [AD A 067 256].

B.5 MILLER, J.F. and INGENITO, F. Normal mode FORTRAN programs for calculating sound propagation in the ocean, Rpt. 3071. Washington, D.C., U.S. Naval Research Laboratory, 1975.

B.6 INGENITO, F., FERRIS, R., KUPERMAN, W.A. and WOLF, S.N. Shallow water acoustics, summary report (first phase), Rpt. 8179. Washington, D.C., U.S. Naval Research Laboratory, 1978.

B.7 JENSEN, F.B. and KUPERMAN, W.A. Environmental acoustical modelling at SACLANTCEN, SACLANTCEN SR-34. La Spezia, Italy, SACLANT ASW Research Centre, 1979. [AD A 081 853].

B.8 FERLA, M.C., DREINI, G., JENSEN, F.B. and KUPERMAN, W.A. Broadband model/data comparisons for acoustic propagation in coastal waters. In: KUPERMAN, W.A. and JENSEN, F.B. eds. Bottom-Interacting Ocean Acoustics. New York, Plenum, 1980: 577-592.

B.9 JENSEN, F.B. Sound propagation in shallow water: a detailed description of the acoustic field close to surface and bottom. Journal Acoustical Society America 70, 1981: 1397-1406.

B.10 TAPPERT, F.D. The parabolic approximation method. In: KELLER, J.B. and PAPADAKIS, J.S. eds. Wave Propagation and Underwater Acoustics. Berlin, Springer-Verlag, 1977: 224-287.

B.11 JENSEN, F.B. and KROL, H.R. The use of the parabolic equation method in sound propagation modelling, SACLANTCEN SM-72. La Spezia, Italy, SACLANT ASW Research Centre, 1975.

B.12 BROCK, H.K. The AESD parabolic equation model, Rpt. TN-12. NSTL Station, Miss., Naval Ocean Research and Development Activity, 1978.

B.13 JENSEN, F.B. and KUPERMAN, W.A. Range-dependent bottom-limited propagation modelling with the parabolic equation. In: KUPERMAN, W.A. and JENSEN, F.B. eds. Bottom-Interacting Ocean Acoustics. New York, Plenum, 1980: 451-466.

B.14 CORNYN, J.J. GRASS: a digital-computer ray-tracing and transmission-loss-prediction system, Rpt. 7621 (Vol. 1, Overall description) and Rpt. 7642 (Vol. 2, User's manual). Washington, D.C., U.S. Naval Research Laboratory, 1973.

# INITIAL DISTRIBUTION

| | Copies |
|---|---|
| **MINISTRIES OF DEFENCE** | |
| MOD Belgium | 2 |
| DND Canada | 10 |
| CHOD Denmark | 8 |
| MOD France | 8 |
| MOD Germany | 15 |
| MOD Greece | 11 |
| MOD Italy | 10 |
| MOD Netherlands | 12 |
| CHOD Norway | 10 |
| MOD Portugal | 5 |
| MOD Turkey | 5 |
| MOD U.K. | 16 |
| SECDEF U.S. | 61 |
| **NATO AUTHORITIES** | |
| Defence Planning Committee | 3 |
| NAMILCOM | 2 |
| SACLANT | 10 |
| SACLANTREPEUR | 1 |
| CINCWESTLANT/COMOCEANLANT | 1 |
| COMIBERLANT | 1 |
| CINCEASTLANT | 1 |
| COMSUBACLANT | 1 |
| COMMAIREASTLANT | 1 |
| SACEUR | 2 |
| CINCNORTH | 1 |
| CINCSOUTH | 1 |
| COMNAVSOUTH | 1 |
| COMSTRIKFORSOUTH | 1 |
| COMEDCENT | 1 |
| COMMARAIRMED | 1 |
| CINCHAN | 1 |

| | Copies |
|---|---|
| **SCNR FOR SACLANTCEN** | |
| SCNR Belgium | 1 |
| SCNR Canada | 1 |
| SCNR Denmark | 1 |
| SCNR Germany | 1 |
| SCNR Greece | 1 |
| SCNR Italy | 1 |
| SCNR Netherlands | 1 |
| SCNR Norway | 1 |
| SCNR Portugal | 1 |
| SCNR Turkey | 1 |
| SCNR U.K. | 1 |
| SCNR U.S. | 2 |
| SECGEN Rep. SCNR | 1 |
| NAMILCOM Rep. SCNR | 1 |
| **NATIONAL LIAISON OFFICERS** | |
| NLO Canada | 1 |
| NLO Denmark | 1 |
| NLO Germany | 1 |
| NLO Italy | 1 |
| NLO U.K. | 1 |
| NLO U.S. | 1 |
| **NLR TO SACLANT** | |
| NLR Belgium | 1 |
| NLR Canada | 1 |
| NLR Denmark | 1 |
| NLR Germany | 1 |
| NLR Greece | 1 |
| NLR Italy | 1 |
| NLR Netherlands | 1 |
| NLR Norway | 1 |
| NLR Portugal | 1 |
| NLR Turkey | 1 |
| NLR UK | 1 |
| NLR US | 1 |
| Total initial distribution | 236 |
| SACLANTCEN Library | 10 |
| Stock | 34 |
| Total number of copies | 280 |